

Data-Driven Linearization of Dynamical Systems

George Haller*and Bálint Kaszás
Institute for Mechanical Systems
ETH Zürich

Leonhardstrasse 21, 8092 Zürich, Switzerland

August 6, 2024

Dynamic Mode Decomposition (DMD) and its variants, such as extended DMD (EDMD), are broadly used to fit simple linear models to dynamical systems known from observable data. As DMD methods work well in several situations but perform poorly in others, a clarification of the assumptions under which DMD is applicable is desirable. Upon closer inspection, existing interpretations of DMD methods based on the Koopman operator are not quite satisfactory: they justify DMD under assumptions that hold only with probability zero for generic observables. Here, we give a justification for DMD as a local, leading-order reduced model for the dominant system dynamics under conditions that hold with probability one for generic observables and non-degenerate observational data. We achieve this for autonomous and for periodically forced systems of finite or infinite dimensions by constructing linearizing transformations for their dominant dynamics within attracting slow spectral submanifolds (SSMs). Our arguments also lead to a new algorithm, data-driven linearization (DDL), which is a higher-order, systematic linearization of the observable dynamics within slow SSMs. We show by examples how DDL outperforms DMD and EDMD on numerical and experimental data.

1 Introduction

In recent years, there has been an overwhelming interest in devising linear models for dynamical systems from experimental or numerical data (see the recent review by Schmid [51]). This trend was largely started by the Dynamic Mode Decomposition (DMD), put forward in seminal work by Schmid [50]. The original exposition of the method has been streamlined by various authors, most notably by Rowley et al. [49] and Kutz et al. [32].

To describe DMD, we consider an autonomous dynamical system

$$\dot{\mathbf{x}} = \mathbf{f}(\mathbf{x}), \quad \mathbf{x} \in \mathbb{R}^n, \quad \mathbf{f} \in C^1(\mathbb{R}^n), \quad (1)$$

for some $n \in \mathbb{N}^+$. Trajectories $\{\mathbf{x}(t; \mathbf{x}_0)\}_{t \in \mathbb{R}}$ of this system evolve from initial conditions \mathbf{x}_0 . The flow map $\mathbf{F}^t: \mathbb{R}^n \rightarrow \mathbb{R}^n$ is defined as the mapping taking the initial trajectory positions at time $t_0 = 0$ to current ones at time t , i.e.,

$$\mathbf{F}^t(\mathbf{x}_0) = \mathbf{x}(t; \mathbf{x}_0). \quad (2)$$

As observations of the full state space variable \mathbf{x} of system (1) are often not available, one may try to explore the dynamical system (1) by observing d smooth scalar functions $\phi_1(x), \dots, \phi_d(x)$ along trajectories of the system. We order these scalar observables into the observable vector

$$\phi(x) = \begin{pmatrix} \phi_1(\mathbf{x}) \\ \vdots \\ \phi_d(\mathbf{x}) \end{pmatrix} \in C^1(\mathbb{R}^n) \quad (3)$$

*Corresponding author. Email: georgehaller@ethz.ch

The basic idea of DMD is to approximate the observed evolution of $\phi(\mathbf{F}^t(\mathbf{x}_0))$ of the dynamical system with the closest fitting autonomous linear dynamical system

$$\dot{\phi} = \mathbf{L}\phi, \quad \mathbf{L} \in \mathbb{R}^{d \times d}, \quad (4)$$

based on available trajectory observations.

This is a challenging objective for multiple reasons. First, the original dynamical system (1) is generally nonlinear whose dynamics cannot be well approximated by a single linear system on a sizable open domain. For instance, one may have several isolated, coexisting attracting or repelling stationary states (such as periodic orbits, limit cycles or quasiperiodic tori), which linear systems cannot have. Second, it is unclear why the dynamics of d observables should be governed by a self-contained autonomous dynamical system induced by the original system (1), whose dimension is n . Third, the result of fitting system (4) to observable data will clearly depend on the initial conditions used, the number and the functional form of the observables chosen, as well as on the objective function used in minimizing the fit.

Despite these challenges, we may proceed to find an appropriately defined closest linear system (4) based on available observable data. We assume that for some fixed time step Δt , discrete observations of m initial conditions, $\mathbf{x}^1(t_0), \dots, \mathbf{x}^m(t_0)$, and their images $\mathbf{F}^{\Delta t}(\mathbf{x}^1(t_0)), \dots, \mathbf{F}^{\Delta t}(\mathbf{x}^m(t_0))$, under the sampled flow map $\mathbf{F}^{\Delta t}$ are available in the data matrices

$$\Phi = [\phi(\mathbf{x}^1(t_0)), \dots, \phi(\mathbf{x}^m(t_0))], \quad \hat{\Phi} = [\phi(\mathbf{F}^{\Delta t}(\mathbf{x}^1(t_0))), \dots, \phi(\mathbf{F}^{\Delta t}(\mathbf{x}^m(t_0)))] , \quad (5)$$

respectively. We seek the best fitting linear system of the form (4) for which

$$\hat{\Phi} \approx \mathcal{D}\Phi, \quad \mathcal{D} = e^{\mathbf{L}\Delta t}, \quad (6)$$

holds. The eigenvalues of such a \mathcal{D} are usually called DMD eigenvalues, and their corresponding eigenvectors are called the DMD modes.

Various norms can be chosen with respect to which the difference of $\hat{\Phi}$ and $\mathcal{D}\Phi$ is to be minimized. The most straightforward choice is the Euclidean matrix norm $|\cdot|$, which leads to the minimization principle

$$\mathcal{D}^* = \operatorname{argmin}_{\mathcal{D} \in \mathbb{R}^{d \times d}} \left| \hat{\Phi} - \mathcal{D}\Phi \right|^2. \quad (7)$$

An explicit solution to this problem is given by

$$\mathcal{D} = \left(\hat{\Phi}\Phi^T \right) \left(\hat{\Phi}\Phi^T \right)^\dagger, \quad (8)$$

with the dagger referring to the pseudo-inverse of a matrix (see, e.g., Kutz et al. [32] for details). We note that the original formulation of Schmid [50] is for discrete dynamical processes and assumes observations of a single trajectory (see also Rowley et al. [49]).

Among several later variants of DMD surveyed by Schmid [51], the most broadly used one is the Extended Dynamic Mode Decomposition (EDMD) of Williams et al. [58]. This procedure seeks the best-fitting linear dynamics for an a priori unknown set of functions $\mathbf{K}(\phi(\mathbf{x}))$ of $\phi(\mathbf{x})$, rather than for $\phi(\mathbf{x})$ itself. In practice, one often chooses \mathbf{K} as an $N(d, k)$ -dimensional vector of d -variate scalar monomials of order k or less, where $N(d, k) = \binom{d+k}{k}$ is the total number of all such monomials. The underlying assumption of EDMD is that a self-contained linear dynamical system of the form

$$\frac{d}{dt} \mathbf{K}(\phi(\mathbf{F}^t(\mathbf{x}_0))) = \mathbf{L}\mathbf{K}(\phi(\mathbf{F}^t(\mathbf{x}_0))) \quad (9)$$

can be obtained on the feature space $\mathbb{R}^{N(d,k)}$ by optimally selecting $\mathbf{L} \in \mathbb{R}^{N(d,k) \times N(d,k)}$. For physical systems, the $N(d, k)$ -dimensional ODE in eq. (9) defined on the feature space $\mathbb{R}^{N(d,k)}$ can be substantially higher-dimensional than the d -dimensional ODE (4). In fact, $N(d, k)$ may be substantially higher than the dimension n of the phase space \mathbb{R}^n of the original nonlinear system (1).

Once the function library used in EDMD is fixed, one again seeks to choose \mathbf{L} so that

$$\mathbf{K}(\hat{\Phi}) \approx \mathcal{D}\mathbf{K}(\Phi), \quad \mathcal{D} = e^{\mathbf{L}\Delta t}.$$

This again leads to a linear optimization problem that can be solved using linear algebra tools. For higher-dimensional systems, a kernel-based version of EDMD was developed by Williams et al. [59]. This method computes inner products necessary for EDMD implicitly, without requiring an explicit representation of (polynomial) basis functions in the space of observables. As a result, kernel-based EDMD operates at computational costs comparable to those of the original DMD.

2 Prior justifications for DMD methods

Available justifications for DMD (see Rowley et al. [49]) and EDMD (see Williams et al. [58]) are based on the Koopman operator, whose basics we review in Appendix A.1 for completeness. The argument starts with the observation that special observables falling in invariant subspaces of this operator in the space of all observables obey linear dynamics. Consequently, DMD should recover the Koopman operator restricted to this subspace if the observables are taken from such a subspace.

In this sense, DMD is viewed as an approximate, continuous immersion of a nonlinear system into an infinite dimensional linear dynamical system. While such an immersion is not possible for typical nonlinear systems with multiple limit sets (see Liu et al. [38, 39]), one still hopes that this approximate immersion is attainable via DMD or EDMD for nonlinear systems with a single attracting steady state that satisfies appropriate nondegeneracy conditions (see Kvalheim and Arathoon [33]). In that case, unlike classic local linearization near fixed points, the linearization via DMD or EDMD is argued to be non-local, as it covers the full domain of definition of Koopman eigenfunctions spanning the underlying Koopman-invariant subspace.

However, Koopman eigenfunctions, whose existence, domain of definition and exact form are a priori unknown for general systems, are notoriously difficult—if not impossible—to determine accurately from data. More importantly, even if Koopman-invariant subspaces of the observable space were known, any countable set of generically chosen observables would lie outside those subspaces with probability one. As a consequence, DMD eigenvectors (which are generally argued to be approximations of Koopman eigenfunctions and can be used to compute Koopman modes¹) would also lie outside Koopman-invariant subspaces, given that such eigenvectors are just linear combinations of the available observables. Consequently, practically observed data sets would fall under the realm of Koopman-based explanation for DMD with probability zero. This is equally true for EDMD, whose flexibility in choosing the function set $\mathbf{K}(\phi(\mathbf{x}))$ of observables also introduces further user-dependent heuristics beyond the dimension d of the DMD.

One may still hope that by enlarging the dimension d of observables in DMD and enlarging the function library $\mathbf{K}(\phi(\mathbf{x}))$ in EDMD, the optimization involved in these methods brings DMD and EDMD eigenvectors closer and closer to Koopman eigenfunctions. The required enlargements, however, may mean hundreds or thousand of dimensions even for dynamical system governed by simple, low-dimensional ODEs (Williams et al. [59]). These enlargements succeed in fitting linear systems closely to sets of observer trajectories, but they also unavoidably lead to overfits that give unreliable predictions for initial conditions not used in the training of DMD or EDMD. Indeed, the resulting large linear systems can perform substantially worse in prediction than much lower dimensional linear or nonlinear models obtained from other data-driven techniques (see, e.g., Alora et al. [1]).

Similar issues arise in justifying the kernel-based EDMD of Williams et al. [59] based on the Koopman operator. Additionally, the choice of the kernel function that represents the inner product of the now implicitly defined polynomial basis functions remains heuristic and problem-dependent.

¹Assuming that each coordinate component x_j of the full phase space vector \mathbf{x} of system (1) falls in a span of the same set of Koopman eigenfunctions $\{\phi_1(\mathbf{x}), \dots, \phi_N(\mathbf{x})\}$, one defines the j^{th} Koopman mode associated with x_j as the vector $\mathbf{v}_j = (v_{1j}, \dots, v_{Nj})^T$ for which $x_j = \sum_{i=1}^N v_{ij}\phi_i(x)$ (see, e.g., Williams et al. [58]).

Again, the accuracy of the procedure is not guaranteed, as available observer data is generically not in a Koopman eigenspace. As Williams et al. [59] write: “Like most existing data-driven methods, there is no guarantee that the kernel approach will produce accurate approximations of even the leading eigenvalues and modes, but it often appears to produce useful sets of modes in practice if the kernel and truncation level of the pseudoinverse are chosen properly.”

Finally, a lesser known limitation of the Koopman-based approach to DMD is the limited domain in the phase space over which Koopman eigenfunctions (and hence their corresponding invariant subspaces) are typically defined in the observable space. Specifically, at least one principal Koopman eigenfunction necessarily blows up near basin boundaries of attracting and repelling fixed points and periodic orbits (see Proposition 1 of our Appendix A.4 for a precise statement and Theorem 3 of Kvalheim and Arathoon [33] for a more general related result).

Expansions of observables in terms of such blowing-up eigenfunctions have even smaller domains of convergence, as was shown explicitly in a simple example by Page and Kerswell [44]. This is a fundamental obstruction to the often envisioned concept of global linear models built of different Koopman eigenfunctions over multiple domains of attraction (see, e.g., Williams et al. [58], p. 1309). While it is broadly known that such models would be discontinuous along basin boundaries (Liu et al. [38, 39], Kvalheim and Arathoon [33]), it is rarely noted (see Kvalheim and Arathoon [33] for such a rare exception) that such models would also generally blow up at those boundaries and hence would become unmanageable even before reaching the boundaries.

For these reasons, an alternative mathematical foundation for DMD is desirable. Ideally, such an approach should be defined on an equal or lower dimensional space, rather than on higher or even infinite-dimensional spaces, as suggested by the Koopman-based view on DMD. This should help in avoiding overfitting and computational difficulties. Additionally, an ideal treatment of DMD should also provide specific non-degeneracy conditions on the underlying dynamical system, on the available observables, and on the specific data to be used in the DMD procedure.

In this paper, we develop a treatment of DMD that satisfies these requirements. This enables to derive conditions for DMD to approximate the dominant linearized observable dynamics near hyperbolic fixed points and periodic orbits of finite- and infinite-dimensional dynamical systems.

Our approach to DMD also leads to a refinement of DMD which we call data-driven linearization (or DDL, for short). DDL effectively carries out exact local linearization via nonlinear coordinate changes on a lower-dimensional attracting invariant manifold (spectral submanifold) of the dynamical system. We illustrate the increased accuracy and domain of validity of DDL models relative to those obtained from DMD and EDMD on examples of autonomous and forced dynamical systems.

3 A simple justification for the DMD algorithm

Here we give an alternative interpretation of DMD and EDMD as approximate models for a dynamical system known through a set of observables. The main idea (to be made more precise shortly) is to view DMD executed on d observables ϕ_1, \dots, ϕ_d as a model reduction tool that captures the leading-order dynamics of $n \geq d$ phase space variables along a d -dimensional slow manifold in terms of ϕ_1, \dots, ϕ_d .

Such manifolds arise as slow spectral submanifolds (SSMs) under weak non-degeneracy assumptions on the linearized spectrum at stable hyperbolic fixed points of the n -dimensional dynamical system (see Cabré et al. [10], Haller and Ponsioen [21], Cenedese et al. [12]). Specifically, a slow SSM $\mathcal{W}(E)$ is tangent to the real eigenspace E spanned by the d slowest decaying linearized modes at the fixed point. If m sample trajectories $\{\mathbf{x}^j(t)\}_{j=1}^m$ are released from a set of initial conditions $\{\mathbf{x}^j(0)\}_{j=1}^m$ at time $t = 0$, then due to their fast decay along the remaining fast spectral subspace F , the $\mathbf{x}^j(t)$ trajectories will become exponentially close to $\mathcal{W}(E)$ by some time $t = t_0 \geq 0$, and closely synchronize with its internal dynamics, as seen in Fig. 1.

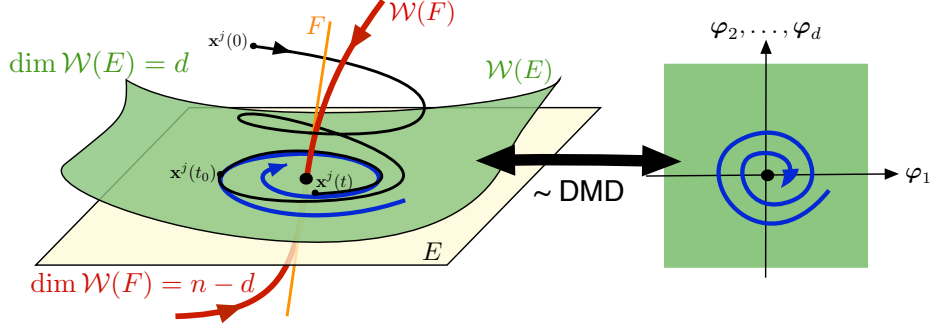


Figure 1: The geometric meaning of DMD performed on d observables, $\phi_1(\mathbf{x}), \dots, \phi_d(\mathbf{x})$, after initial fast transients die out at an exponential rate in the data. DMD then identifies the leading-order (linear) dynamics on a d -dimensional attracting spectral submanifold (SSM) $\mathcal{W}(E)$ tangent to the d -dimensional slow spectral subspace E . These linearized dynamics can be expressed in terms of the SSM-restricted observables $\boldsymbol{\varphi} = \boldsymbol{\phi}|_{\mathcal{W}(E)}$. Also shown is the spectral subspace F of the faster decaying modes and its associated nonlinear continuation, the fast spectral subspace $\mathcal{W}(F)$.

If $\mathcal{W}(E)$ admits a non-degenerate parametrization with respect to the observables ϕ_1, \dots, ϕ_d , then one can pass to these observables as new coordinates in which to approximate the leading order, linearized dynamics inside $\mathcal{W}(E)$. Specifically, DMD executed over time the interval $[t_0, t_0 + \Delta t]$ provides the closest linear fit to the reduced dynamics of $\mathcal{W}(E)$ from the available observable histories $\phi_1(\mathbf{x}^j(t)), \dots, \phi_d(\mathbf{x}^j(t))$ for $t \in [t_0, t_0 + \Delta t]$, as illustrated in Fig. 1. This fit is a close representation of the actual linearized dynamics on the SSM $\mathcal{W}(E)$ if the trajectory data $\{\mathbf{x}^j(t)\}_{j=1}^m$ is sufficiently diverse for $t \geq t_0$. The resulting DMD model with coefficient matrix \mathcal{D} will then be smoothly conjugate to the linearized reduced dynamics on $\mathcal{W}(E)$ with an error of the order of the distance of $\{\mathbf{x}^j(t)\}_{j=1}^m$ from $\mathcal{W}(E)$ between the times t_0 and $t_0 + \Delta t$.

The slow SSM $\mathcal{W}(E)$ may also contain unstable modes in applications. Similar results hold for that case as well, provided that we select a small enough Δt , ensuring that the trajectories $\{\mathbf{x}^j(0)\}_{j=1}^m$ are not ejected from the vicinity of the fixed point origin for $t \in [t_0, t_0 + \Delta t]$. As DMD will show sensitivity with respect to the choice of t_0 and Δt in this case, we will not discuss the justification of DMD near unstable fixed points beyond Remarks 1 and 7.

In the following sections, we make this basic idea more precise both for finite and infinite-dimensional dynamical systems. This approach also reveals explicit, previously undocumented non-degeneracy conditions on the underlying dynamical system, on the available observable functions and on the specific data set used, under which DMD should give meaningful results.

3.1 Justification of DMD for continuous dynamical systems

We start by assuming that the observed dynamics take place in a domain containing a fixed point, which is assumed to be at the origin, without loss of generality, i.e.,

$$\mathbf{f}(\mathbf{0}) = \mathbf{0}. \quad (10)$$

We can then rewrite the dynamical system (1) in the more specific form

$$\dot{\mathbf{x}} = \mathbf{A}\mathbf{x} + \tilde{\mathbf{f}}(\mathbf{x}), \quad \mathbf{x} \in \mathbb{R}^n, \quad \mathbf{A} = D\mathbf{f}(\mathbf{0}), \quad \tilde{\mathbf{f}}(\mathbf{x}) = o(|\mathbf{x}|), \quad (11)$$

where the classic $o(|\mathbf{x}|)$ notation refers to the fact that $\lim_{\mathbf{x} \rightarrow \mathbf{0}} \left[\frac{|\tilde{\mathbf{f}}(\mathbf{x})|}{|\mathbf{x}|} \right] = 0$.

Most expositions of DMD methods and their variants do not state assumption (10) explicitly and hence may appear less restrictive than our treatment here. However, all of them implicitly assume the existence of such a fixed point, as all of them end up returning homogeneous linear ODEs or

mappings with a fixed point at the origin. Indeed, all known applications of these methods that produce reasonable accuracy target the dynamics of ODEs or discrete maps near their fixed points.

Assumption (10) can be replaced with the existence of a limit cycle in the original system (1), in which case the first return map (or Poincaré map) defined near the limit cycle will have a fixed point. We give a separate treatment on justifying DMD as a linearization for such a Poincaré map in Section 3.2.

We do not advocate, however, the often used procedure of applying DMD to fit a linear system to the flow map (rather than the Poincaré map) near a stable limit cycle. Such a fit only produces the desired limiting periodic behavior if one or more of the DMD eigenvalues are artificially constrained to be on the complex unit circle by the user of DMD. This renders the DMD model both structurally unstable and conceptually inaccurate for prediction. Indeed, the model will approximate the originally observed limit cycle and convergence to it only within a measure zero, cylindrical set of its phase space. Outside this set, all trajectories of the DMD model will converge to some other member of the infinite family of periodic orbits or invariant tori within the center subspace corresponding to the unitary eigenvalues. These periodic orbits or tori have a continuous range of locations and amplitudes, and hence represent spurious asymptotic behaviors that are not seen in the original dynamical system (1).

In the special case of $d = n$ and for the special observable $\phi(x) = \mathbf{x}$, the near-linear form of eq. (11) motivates the DMD procedure because a linear approximation to the system near $\mathbf{x} = \mathbf{0}$ seems feasible. It is a priori unclear, however, to what extent the nonlinearities distort the linear dynamics and how DMD would account for that. Additionally, in a data-driven analysis, choosing the full phase space variable \mathbf{x} as the observable $\phi(\mathbf{x})$ is generally unrealistic. For these reasons, a mathematical justification of DMD requires further assumptions, as we discuss next.

Let $\lambda_1, \dots, \lambda_n \in \mathbb{C}$ denote the eigenvalues of A and let $\mathbf{e}_1, \dots, \mathbf{e}_n \in \mathbb{C}^n$ denote the corresponding generalized eigenvectors. We assume that at least one of the modes of the linearized system at $\mathbf{x} = \mathbf{0}$ decays exponentially and there is at least one other mode that decays slower or even grows. More specifically, for some positive integer $d < n$, we assume that the spectrum of A can be partitioned as

$$\operatorname{Re}\lambda_n \leq \dots \leq \operatorname{Re}\lambda_{d+1} < \operatorname{Re}\lambda_d \leq \dots \leq \operatorname{Re}\lambda_1 < 0. \quad (12)$$

This guarantees the existence of a d -dimensional, normally attracting *slow spectral subspace*

$$E = \operatorname{span} \{\operatorname{Re} \mathbf{e}_1, \operatorname{Im} \mathbf{e}_1, \dots, \operatorname{Re} \mathbf{e}_d, \operatorname{Im} \mathbf{e}_d\} \quad (13)$$

for the linearized dynamics, with linear decay rate towards E strictly dominating all decay rates inside E . Note that the set of vectors $\operatorname{Re} \mathbf{e}_1, \operatorname{Im} \mathbf{e}_1, \dots, \operatorname{Re} \mathbf{e}_d, \operatorname{Im} \mathbf{e}_d$ is, in general, not linearly independent, but they span a d -dimensional subspace. We also define the (real) spectral subspace of faster decaying linear modes:

$$F = \operatorname{span} \{\operatorname{Re} \mathbf{e}_{d+1}, \operatorname{Im} \mathbf{e}_{d+1}, \dots, \operatorname{Re} \mathbf{e}_n, \operatorname{Im} \mathbf{e}_n\}. \quad (14)$$

We will also use matrices containing the left and right eigenvectors of the operator \mathbf{A} and of its restrictions, $\mathbf{A}|_E$ and $\mathbf{A}|_F$, to its spectral subspaces E and F , respectively. Specifically, we let

$$\mathbf{T} = [\mathbf{T}_E, \mathbf{T}_F], \quad \mathbf{P} = \begin{bmatrix} \mathbf{P}_E \\ \mathbf{P}_F \end{bmatrix}, \quad (15)$$

where the columns of $\mathbf{T}_E \in \mathbb{R}^{n \times d}$ are the real and imaginary parts of the generalized right eigenvectors of $\mathbf{A}|_E$ and the columns of $\mathbf{T}_F \in \mathbb{R}^{n \times (n-d)}$ are defined analogously for $\mathbf{A}|_F$. Similarly, the rows of $\mathbf{P}_E \in \mathbb{R}^{d \times n}$ are the real and imaginary parts of the generalized left eigenvectors of $\mathbf{A}|_E$ and the rows of $\mathbf{P}_F \in \mathbb{R}^{(n-d) \times d}$ are defined analogously for $\mathbf{A}|_F$. Under assumption (12), F is always a fast spectral subspace, containing all trajectories of the linearized system that decay faster to the origin as any trajectory in E .

We will use the notation

$$\mathbf{X} = [\mathbf{x}^1(t_0), \dots, \mathbf{x}^m(t_0)], \quad \hat{\mathbf{X}} = [\mathbf{F}^{\Delta t}(\mathbf{x}^1(t_0)), \dots, \mathbf{F}^{\Delta t}(\mathbf{x}^m(t_0))] \quad (16)$$

for trajectory data in the underlying dynamical system ((1)) on which the observable data matrices Φ and $\hat{\Phi}$ defined in (5) are defined. In truly data-driven applications, the matrices \mathbf{X} and $\hat{\mathbf{X}}$ are not known. We will nevertheless use them to make precise statements about a required dominance of the slow linear modes of E in the available data. Such a dominance will arise for generic initial conditions if one selects the initial conditions $\mathbf{x}^1(t_0), \dots, \mathbf{x}^m(t_0)$ after initial fast transients along F have died out. This can be practically achieved by initializing $\mathbf{x}^1(t_0), \dots, \mathbf{x}^m(t_0)$ after a linear spectral analysis of the observable data matrix Φ only returns a number of dominant frequencies consistent with a d -dimensional SSM.

We now state a theorem that provides a general justification for the DMD procedure under explicit nondegeneracy conditions and with specific error bounds. Specifically, we give a minimal set of conditions under which DMD can be justified as an approximate, leading-order, d -dimensional reduced-order model for a nonlinear system of dimension $n \geq d$ near its fixed point. Based on relevance for applications, we only state Theorem 1 for stable hyperbolic fixed points, but discuss subsequently in Remark 1 its extension to unstable fixed points.

Theorem 1. [Justification of DMD for ODEs with stable hyperbolic fixed points] Assume that

(A1) *The $\mathbf{x} = \mathbf{0}$ is a stable hyperbolic fixed point of system (11) with a spectral gap, i.e., the spectrum $\text{Spect}[\mathbf{A}]$ satisfies eq. (12).*

(A2) *$\mathbf{f} \in C^2$ in a neighborhood of the origin.*

(A3) *For some integer $d \in [1, n]$, a d -dimensional observable function $\phi \in C^2$ and the d -dimensional slow spectral subspace E of the hyperbolic fixed point $\mathbf{x} = \mathbf{0}$ of system (11) satisfy the non-degeneracy condition*

$$\text{rank}[D\phi(\mathbf{0})|_E] = d. \quad (17)$$

(A4) *The data matrices Φ and $\hat{\Phi}$ are non-degenerate and the initial conditions in \mathbf{X} and $\hat{\mathbf{X}}$ have been selected after fast transients from the modes outside E have largely died out, i.e.,*

$$\text{rank}_{\text{row}} \Phi = d, \quad |\mathbf{P}_F \mathbf{X}|, |\mathbf{P}_F \hat{\mathbf{X}}| \leq |\mathbf{P}_E \mathbf{X}|^{1+\beta}, \quad (18)$$

for some $\beta \in (0, 1]$.

Then the DMD computed from Φ and $\hat{\Phi}$ yields a matrix \mathcal{D} that is locally topologically conjugate with order $\mathcal{O}(|\mathbf{P}_E \mathbf{X}|^\beta)$ error to the linearized dynamics on a d -dimensional, slow attracting spectral submanifold $\mathcal{W}(E) \in C^1$ tangent to E at $\mathbf{x} = \mathbf{0}$. Specifically, we have

$$\mathcal{D} = D\phi(\mathbf{0})\mathbf{T}_E e^{\Lambda_E \Delta t} (D\phi(\mathbf{0})\mathbf{T}_E)^{-1} + \mathcal{O}(|\mathbf{P}_E \mathbf{X}|^\beta). \quad (19)$$

Proof. Under assumptions (A1) and (A2), any trajectory in a neighborhood of the origin in the nonlinear system (11) converges at an exponential rate $e^{\text{Re}\lambda_{d+1} t}$ to a d -dimensional attracting spectral submanifold $\mathcal{W}(E)$ tangent to a d -dimensional attracting slow spectral subspace E of the linearized system at the origin. This follows from the C^1 linearization theorem of Hartman [23], which is applicable to C^2 dynamical systems with a stable hyperbolic fixed point. Under assumption (A3), the d -dimensional observable function $\phi(\mathbf{x})$ restricted to $\mathcal{W}(E)$ can be used to parametrize $\mathcal{W}(E)$ near the origin, and hence a d -dimensional, self-contained nonlinear dynamical system can be written down for the restricted observable $\varphi = \phi|_{\mathcal{W}(E)}$ along $\mathcal{W}(E)$. Under the first assumption in

(A4), the available observational data matrices Φ and $\hat{\Phi}$ are rich enough to characterize the reduced dynamics on $\mathcal{W}(E)$. Under the second assumption in (A4), transients from the faster modes outside E have largely died out before the selection of the initial conditions in \mathbf{X} , so that the linear part of the dynamics on $\mathcal{W}(E)$ can be approximately inferred from Φ and $\hat{\Phi}$. In that case, up to an error proportional to the distance of the training data from $\mathcal{W}(E)$, the matrix $\mathcal{D} \in \mathbb{R}^{d \times d}$ returned by DMD is similar to the time- Δt flow map of the linearized flow of the underlying dynamical system restricted to $\mathcal{W}(E)$. This linearized flow then acts as a local reduced-order model with which nearby trajectory observations synchronize exponentially fast in the observable space. We give a more detailed proof of the theorem in Appendix (B). \square

Remark 1. In Theorem 1, we can replace assumption (A1) with

$$\operatorname{Re}\lambda_n \leq \dots \leq \operatorname{Re}\lambda_{d+1} < 0, \quad \operatorname{Re}\lambda_{d+1} < \operatorname{Re}\lambda_d \leq \dots \leq \operatorname{Re}\lambda_1, \quad \operatorname{Re}\lambda_j \neq 0, \quad j = 1, \dots, n. \quad (20)$$

This means that the $\mathbf{x} = \mathbf{0}$ fixed point is only assumed hyperbolic with a spectral gap and \mathbf{A} has an attracting d -dimensional spectral subspace E that possibly contains some instabilities, i.e., eigenvalues with positive real parts. Then the statements of Theorem 1 still hold, but $\mathcal{W}(E)$ will only be guaranteed C^1 at $\mathbf{x} = \mathbf{0}$ and Hölder-continuous at other points near the fixed point. This follows by replacing the linearization theorem of Hartman [23] with that of van Strien [56], which still enables us to use eq. (79) in the proof. Therefore, slow subspaces E containing a mixture of stable and unstable modes can also be allowed, as long as F contains only fast modes consistent with the splitting assume in eq. (12). In that case, however, the time $t_0 + \Delta t$ must be chosen carefully to ensure that $|\mathbf{P}_F \hat{\mathbf{X}}| \leq |\mathbf{P}_E \mathbf{X}|^{1+\beta}$ still holds, i.e., the data used in DMD still samples a neighborhood of the origin.

Remark 2. In related work, Boltt et al. [7] construct the transformation relating a pair of conjugate dynamical systems based on a limited set of matching Koopman eigenfunctions, which are either known explicitly or constructed from EDMD with dictionary learning (EDMD-DL; see Li et al. [36]). In principle, this could be used to construct linearizing transformation as well. However, even when the eigenfunctions are approximated from data, the approach assumes that the linearized system, as well as a linearized trajectory and its preimage under the linearization, are available. As these assumptions are not satisfied in practice, only very simple and low-dimensional analytic examples are treated by Boltt et al. [7].

In Appendix (B), Remarks 4-5 summarize technical points on the application and possible further extensions of Theorem 1. In practice, Theorem 1 provides previously unspecified non-degeneracy conditions on the linear part of the dynamical system to be analyzed via DMD (assumption (A1)), on the regularity of the nonlinear part of the system (assumption (A2)), on the type of observables available for the analysis (assumption (A3)) and on the specific observable data used in the analysis (assumption (A4)). The latter assumption requires that there have to be at least as many independent observations in time as observables. This specifically excludes the popular use of tall Φ observable data matrices which provide more free parameters to pattern-match observational data but will also lead to an overfit that diminishes the predictive power of the DMD model on initial conditions not used in its training.

To illustrate these points, we demonstrate the necessity of assumptions (A2)-(A4) of Theorem 1 in Appendix C on simple examples.

3.2 Justification of DMD for discrete and for time-periodic continuous dynamical systems

The linearization results we have applied to deduce Theorem 1 are equally valid for discrete dynamical systems defined by iterated mappings. Such mappings are of the form

$$\mathbf{x}_{n+1} = \mathbf{f}(\mathbf{x}_n) = \mathbf{A}\mathbf{x}_n + \tilde{\mathbf{f}}(\mathbf{x}_n), \quad \mathbf{x}_j \in \mathbb{R}^n, \quad \mathbf{A} \in \mathbb{R}^{n \times n}, \quad \tilde{\mathbf{f}}(\mathbf{x}) = o(|\mathbf{x}|). \quad (21)$$

We will use a similar ordering for the eigenvalues of \mathbf{A} as in the continuous time case:

$$|\lambda_n| \leq \dots \leq |\lambda_{d+1}| < |\lambda_d| \leq \dots \leq |\lambda_1| < 1. \quad (22)$$

As in the continuous time case, we will use the observable data matrices

$$\mathbf{\Phi} = \phi(\mathbf{X}), \quad \hat{\mathbf{\Phi}} = \phi(\mathbf{f}(\mathbf{X})), \quad (23)$$

with the initial conditions for the map \mathbf{f} stored in \mathbf{X} .

With these ingredients, we need only minor modifications in the assumptions of the theorems that account for the usual differences between the spectrum of an ODE and a map.

Theorem 2. [Justification of DMD for maps with stable hyperbolic fixed points] Assume that

(A1) $\mathbf{x} = \mathbf{0}$ is a stable hyperbolic fixed point of system (21), i.e., assumption (22) holds.

(A2) In eq. (21), $\tilde{\mathbf{f}} \in C^2$ holds in a neighborhood of the origin.

(A3) For some integer $d \in [1, n]$, a d -dimensional observable function $\phi \in C^2$ and the d -dimensional slow spectral subspace E of the hyperbolic fixed point $\mathbf{x} = \mathbf{0}$ of system (21) satisfy the non-degeneracy condition

$$\text{rank } [D\phi(\mathbf{0})|_E] = d. \quad (24)$$

(A4) The data matrices $\mathbf{\Phi}$ and $\hat{\mathbf{\Phi}}$ collected from iterations of system (21) are non-degenerate and are dominated by data near E , i.e.,

$$\text{rank}_{\text{row}} \mathbf{\Phi} = d, \quad |\mathbf{P}_F \mathbf{X}|, |\mathbf{P}_F \hat{\mathbf{X}}| \leq |\mathbf{P}_E \mathbf{X}|^{1+\beta}, \quad (25)$$

for some $\beta \in (0, 1)$.

Then the DMD computed from $\mathbf{\Phi}$ and $\hat{\mathbf{\Phi}}$ yields a matrix \mathcal{D} that is locally topologically conjugate with order $\mathcal{O}(|\mathbf{P}_E \mathbf{X}|^\beta)$ error to the linearized dynamics on a d -dimensional attracting spectral submanifold $\mathcal{W}(E) \in C^1$ tangent to E at $\mathbf{x} = \mathbf{0}$. Specifically, we have

$$\mathcal{D} = D\phi(\mathbf{0})\mathbf{T}_E\mathbf{\Lambda}_E(D\phi(\mathbf{0})\mathbf{T}_E)^{-1} + \mathcal{O}(|\mathbf{P}_E \mathbf{X}|^\beta). \quad (26)$$

The spectral submanifold $\mathcal{W}(E)$ and its reduced dynamics are of class C^1 at the origin, and at least Hölder continuous in a neighborhood of the origin.

Proof. The proof is identical to the proof of Theorem 1 but uses the discrete version of the linearization result by Hartman [23] for stable hyperbolic fixed points of maps. \square

Theorem 1 can be immediately applied to justify DMD as a linearization tool for period-one maps (or Poincaré maps) of time-periodic, non-autonomous dynamical systems near their periodic orbits. This requires the data matrices $\mathbf{\Phi}$ and $\hat{\mathbf{\Phi}}$ to contain trajectories of such a Poincaré map. Remark 8 on the treatment of slow spectral subspaces E containing possible instabilities also applies here under the modified assumption

$$|\lambda_n| \leq \dots \leq |\lambda_{d+1}| < 1, \quad |\lambda_{d+1}| < |\lambda_d| \leq \dots \leq |\lambda_1|, \quad |\lambda_j| \neq 1, \quad j = 1, \dots, n, \quad (27)$$

which only requires the fixed point to be hyperbolic and \mathbf{A} to have a d -dimensional normally attracting subspace.

3.3 Justification of DMD for infinite-dimensional dynamical systems

Most data sets of interest arguably arise from infinite-dimensional dynamical systems of fluids and solids. Examples include experimental or numerical data describing fluid motion, continuum vibrations, climate dynamics or salinity distribution in the ocean. In the absence of external forcing, these problems are governed by systems of autonomous nonlinear partial differential equations that can often be viewed as evolutionary differential equations in a form similar to eq. (1), but defined on an appropriate infinite-dimensional Banach space. Accordingly, time-sampled solutions of these equations can be viewed as iterated mappings of the form (21) but defined on Banach spaces.

Our approach to justifying DMD generally carries over to this infinite-dimensional setting, as long as the observable vector $\phi(\mathbf{x})$ remains finite-dimensional, and both the Banach space and the discrete or continuous dynamical system defined on it satisfy appropriate regularity conditions. These regularity conditions tend to be technical, but when they are satisfied, they do guarantee the extension of Theorems 1-2 to Banach spaces. This offers a justification to use DMD to obtain an approximate finite-dimensional linear model for the dynamics of the underlying continuum system on a finite-dimensional attracting slow manifold (or inertial manifold) in the neighborhood of a non-degenerate stationary solution.

To avoid major technicalities, we only state here a generalized version of Theorem 1 to justify the use of DMD for observables defined on Banach spaces for a discrete evolutionary process with a stable hyperbolic stationary state. We consider mappings of the form

$$\mathbf{x}_{n+1} = \mathbf{f}(\mathbf{x}_n) = \mathbf{A}\mathbf{x}_n + \tilde{\mathbf{f}}(\mathbf{x}_n), \quad \mathbf{x}_j \in \mathcal{B}, \quad \tilde{\mathbf{f}}: U \subset \mathcal{B} \rightarrow \mathcal{B}, \quad \tilde{\mathbf{f}}(\mathbf{0}) = \mathbf{0} \in U, \quad (28)$$

where \mathcal{B} is a Banach space, U is an open set in \mathcal{B} , and $\mathbf{A}: \mathcal{B} \rightarrow \mathcal{B}$ is an invertible linear operator that is bounded in the norm defined on \mathcal{B} . The function \mathbf{f} can be here the time-sampled version of an infinite-dimensional flow map of an autonomous evolutionary PDE or the Poincaré map of a time-periodic evolutionary PDE. We assume that for some $\alpha \in (0, 1)$, $\tilde{\mathbf{f}} \in C^{1,\alpha}(U)$ holds, i.e., $\tilde{\mathbf{f}}$ is (Fréchet-) differentiable in U and its derivative, $D\tilde{\mathbf{f}}$, is Hölder-continuous in $\mathbf{x} \in U$ with Hölder exponent α .

The *spectral radius* of A is defined as

$$\rho(\mathbf{A}) = \lim_{k \rightarrow \infty} |\mathbf{A}^k|^{\frac{1}{k}}.$$

We recall that in the special case $\mathcal{B} = \mathbb{R}^n$ treated in Section 3.2, we have $\rho(\mathbf{A}) = \max_{1 \leq j \leq n} |\lambda_j|$. For some $\alpha \in (0, 1)$, the linear operator \mathbf{A} is called α -*contracting* if

$$\rho(\mathbf{A})^{1+\alpha} \rho(\mathbf{A}^{-1}) < 1, \quad (29)$$

which can only hold if $\rho(\mathbf{A}) < 1$ (see Newhouse [41]). Therefore, in the simple case of $\mathcal{B} = \mathbb{R}^n$, A is α -*contracting* if it is a contraction (i.e., all its eigenvalues are less than one in norm) and

$$|\lambda_1|^{1+\alpha} < |\lambda_n|,$$

showing that the spectrum of \mathbf{A} is confined to an annulus of outer radius $|\lambda_1| < 1$ and inner radius $|\lambda_1|^{1+\alpha}$. We can now state our main result on the justification of DMD for infinite-dimensional discrete dynamical systems.

Theorem 3. [Justification of DMD for infinite-dimensional maps with stable hyperbolic fixed points] Assume that

(A1) For some $\alpha \in (0, 1)$, the linear operator \mathbf{A} is α -*contracting* (and hence the $x = 0$ fixed point of system (28) is linearly stable).

(A2) In eq. (28), $\tilde{\mathbf{f}} \in C^{1,\alpha}(U)$ holds in a U neighborhood of the origin.

(A3) For some integer $d \in \mathbb{N}^+$, there is a splitting $\mathcal{B} = E \oplus F$ of \mathcal{B} into two A -invariant subspaces $E, F \subset \mathcal{B}$ such that E is d -dimensional and slow, i.e.,

$$\rho(\mathbf{A}|_E) < \frac{1}{\rho(\mathbf{A}^{-1}|_F)} \quad (30)$$

Furthermore, a d -dimensional observable function $\phi \in C^2$ satisfies the non-degeneracy condition

$$\text{rank } [D\phi(\mathbf{0})|_E] = d. \quad (31)$$

(A4) The data matrices Φ and $\hat{\Phi}$ collected from iterations of system (28) are non-degenerate and are dominated by data near E , i.e.,

$$\text{rank}_{\text{row}} \Phi = d, \quad |\mathbf{P}_F \mathbf{X}|, |\mathbf{P}_F \hat{\mathbf{X}}| \leq |\mathbf{P}_E \mathbf{X}|^{1+\beta}, \quad (32)$$

for some $\beta \in (0, 1)$.

Then the DMD computed from Φ and $\hat{\Phi}$ yields a matrix \mathcal{D} that is locally topologically conjugate with order $\mathcal{O}(|\mathbf{P}_E \mathbf{X}|^\beta)$ error to the linearized dynamics on a d -dimensional attracting spectral submanifold $\mathcal{W}(E)$ tangent to E at $\mathbf{x} = \mathbf{0}$. Specifically, we have

$$\mathcal{D} = D\phi(\mathbf{0})\mathbf{T}_E\mathbf{\Lambda}_E(D\phi(\mathbf{0})\mathbf{T}_E)^{-1} + \mathcal{O}(|\mathbf{P}_E \mathbf{X}|^\beta). \quad (33)$$

The spectral submanifold $\mathcal{W}(E)$ and its reduced dynamics are of class C^1 in a neighborhood of the origin.

Proof. The proof follows the steps in the proof of Theorem 2 but uses an infinite-dimensional linearization result, Theorem 3.1 of Newhouse [41], for stable hyperbolic fixed points of maps on Banach spaces. Specifically, if \mathbf{A} is α -contracting, then Newhouse [41] shows the existence of a near-identity linearizing transformation $\mathbf{x} = \mathbf{y} + \mathbf{h}(\mathbf{y})$ for the discrete dynamical system (28) such that $\mathbf{h} \in C^{1,\alpha}(B)$ holds on a small enough ball $B \subset U$ centered at $\mathbf{x} = \mathbf{0}$. Using this linearization theorem instead of its finite-dimensional version from Hartman [23], we can follow the same steps as in the proof of Theorem 2 to conclude the statement of the theorem. \square

In Appendix B, Remarks 6-7 summarize technical remarks on possible further extensions of Theorem 3.

4 Data-Driven Linearization (DDL)

4.1 Theoretical foundation for DDL

Based on the results of the previous section, we now refine the first-order approximation to the linearized dynamics yielded by DMD near a hyperbolic fixed point. Specifically, we construct the specific nonlinear coordinate change that linearizes the restricted dynamics on the attracting spectral submanifold $\mathcal{W}(E)$ illustrated in Fig. 1. This classic notion of linearization on $\mathcal{W}(E)$ yields a d -dimensional linear reduced model, which can be of significantly lower dimension than the original n -dimensional nonlinear system. This is to be contrasted with the broadly pursued Koopman embedding approach (see, e.g., Rowley et al. [49], Budišić et al. [8], Mezić [40]), which seeks to immerse nonlinear systems into linear systems of dimensions substantially higher (or even infinite) relative to n .

The following result gives the theoretical basis for our subsequent data-driven linearization (DDL) algorithm. We will use the notation C^a for the class of real analytic functions.

Theorem 4. [DDL principle for ODEs with a stable hyperbolic fixed points] Assume that the $\mathbf{x} = \mathbf{0}$ stable hyperbolic fixed point of system (11) and the spectrum of \mathbf{A} has a spectral gap as in eq. (12). Assume further that for some $r \in \mathbb{N}^+ \cup \{\infty, a\}$, the following conditions are satisfied:

(B1) $\mathbf{f}_2 \in C^r$ and for all nonnegative integers m_j , the nonresonance conditions

$$\lambda_k \neq \sum_{j=1}^n m_j \lambda_j, \quad k = 1, \dots, n, \quad 2 \leq \sum_{j=1}^n m_j \leq Q \leq r, \quad Q := \left\lceil \frac{\max_i |\operatorname{Re} \lambda_i|}{\min_i |\operatorname{Re} \lambda_i|} \right\rceil + 1, \quad (34)$$

hold for the eigenvalues of \mathbf{A} , with $\lceil \cdot \rceil$ referring to the integer part of a positive number.

(B2) For some integer $d \in [1, n]$, a d -dimensional observable function $\phi \in C^r$ and the d -dimensional slow spectral subspace E of the stable fixed point $\mathbf{x} = \mathbf{0}$ of system (11) satisfy the non-degeneracy condition.

$$\operatorname{rank} [D\phi(\mathbf{0})|_E] = d. \quad (35)$$

Then the following hold:

(i) On the unique d -dimensional attracting spectral submanifold $\mathcal{W}(E) \in C^r$ tangent to E at $x = 0$, the reduced observable vector $\varphi = \phi|_{\mathcal{W}(E)}$ can be used to describe the reduced dynamics as

$$\dot{\varphi} = \mathbf{B}\varphi + \mathbf{q}(\varphi), \quad \mathbf{B} = D\phi(\mathbf{0})\mathbf{T}_E\mathbf{A}_E(D\phi(\mathbf{0})\mathbf{T}_E)^{-1}, \quad \mathbf{q}(\varphi) = \mathcal{O}(|\varphi|^2). \quad (36)$$

(ii) There exists a unique, C^r change of coordinates

$$\varphi = \kappa(\gamma) = \gamma + \ell(\gamma), \quad (37)$$

that transforms the reduced dynamics on $\mathcal{W}(E)$ to its linearization

$$\dot{\gamma} = \mathbf{B}\gamma \quad (38)$$

inside the domain of attraction of $\mathbf{x} = \mathbf{0}$ within the spectral submanifold $\mathcal{W}(E)$.

(iii) The transformation (37) satisfies the d -dimensional system of nonlinear PDEs

$$D_\gamma \ell(\gamma)\mathbf{B}\gamma = \mathbf{B}\ell(\gamma) + \mathbf{q}(\gamma + \ell(\gamma)). \quad (39)$$

If $r \in \mathbb{N}^+ \cup \{\infty\}$, solutions of this PDE can locally be approximated as

$$\ell(\gamma) = \sum_{|\mathbf{k}|=2}^r \mathbf{l}_\mathbf{k} \gamma^\mathbf{k} + o(|\gamma|^r), \quad \mathbf{k} \in \mathbb{N}^d, \quad \mathbf{l}_\mathbf{k} \in \mathbb{R}^d, \quad \gamma^\mathbf{k} := \gamma_1^{k_1} \dots \gamma_d^{k_d}. \quad (40)$$

If $r = a$, then the local approximation (40) can be refined to a convergent Taylor series

$$\ell(\gamma) = \sum_{|\mathbf{k}|=2}^{\infty} \mathbf{l}_\mathbf{k} \gamma^\mathbf{k}, \quad \mathbf{k} \in \mathbb{N}^d, \quad \mathbf{l}_\mathbf{k} \in \mathbb{R}^d, \quad \gamma^\mathbf{k} := \gamma_1^{k_1} \dots \gamma_d^{k_d} \quad (41)$$

in a neighborhood of the origin. In either case, the coefficients $\mathbf{l}_\mathbf{k}$ can be determined by substituting the expansion for $\ell(\gamma)$ into the PDE (39), equating coefficients of equal monomials $\gamma^\mathbf{k}$ and solving the corresponding recursive sequence of d -dimensional linear algebraic equations for increasing $|\mathbf{k}|$.

Proof. The proof builds on the existence of the d -dimensional spectral submanifold $\mathcal{W}(E)$ guaranteed by Theorem 1. For a C^r dynamical system with $r \in \mathbb{N}^+ \cup \{\infty, a\}$, $\mathcal{W}(E)$ is also C^r smooth based on the linearization theorems of Poincaré [46] and Sternberg [52], as long as the nonresonance condition (34) holds. Condition (35) then ensures that $\mathcal{W}(E)$ can be parametrized locally by the restricted

observable vector φ and hence its reduced dynamics can be written as a nonlinear ODE for φ . This ODE can again be linearized by a near-identity coordinate change (37) using the appropriate linearization theorem of the two cited above. The result is the restricted linear system (38) to which the dynamics is C^r conjugate within the whole domain of attraction of the $\varphi = \mathbf{0}$ fixed point inside $\mathcal{W}(E)$. The invariance PDE (39) can be obtained by substituting the linearizing transformation (37) into the reduced dynamics on $\mathcal{W}(E)$. This PDE can then be solved via a Taylor expansion up to order r . We give more a more detailed proof in Appendix D. \square

Note that 1 : 1 resonances are not excluded by the condition (34), and hence repeated eigenvalues arising from symmetries in physical systems are still amenable to DDL. Also of note is that the non-resonance conditions (34) do not exclude frequency-type resonances among imaginary parts of oscillatory eigenvalues. Rather, they exclude simultaneous resonances of the same type between the real and the imaginary parts of the eigenvalues. Such resonances will be absent in data generated by generic oscillatory systems.

Assuming hyperbolicity is essential for Theorem 4 to hold, since in this case the linearization is the same as transforming the dynamics to the Poincaré-normal form. For a non-hyperbolic fixed point, this normal form transformation results in nonlinear dynamics on the center manifold. This would, however, only arise in highly non-generic systems, precisely tuned to be at criticality. Since this is unlikely to happen in experimentally observed or numerically simulated systems, the hyperbolicity assumption is not restrictive.

Finally, under the conditions of Theorem 3, the DDL results of Theorem 4 also apply to data from infinite-dimensional dynamical systems, such as the fluid sloshing experiments we will analyze using DDL in Section 5.4. In practice, the most restrictive condition of Theorem 3 is (A1), which requires the solution operator to have a spectrum uniformly bounded away from zero. Such uniform boundedness is formally violated in important classes of infinite-dimensional evolution equations, presenting a technical challenge for the direct applications of SSM results to certain delay-differential equations (see Szaksz [54]) and partial differential equations (see, e.g., Kogelbauer and Haller [30] and Buza [9]). However, this challenge only concerns rigorous conclusions on the existence and smoothness of a finite-dimensional, attracting SSM. If the existence of such an SSM is convincingly established from an alternative mathematical theory (as is Buza [9]) or inferred from data (as in Szaksz [54]), then the DDL algorithm based on Theorem 4 can be used to obtain a data-driven linearization of the dynamics on that SSM.

4.2 DDL vs. EDMD

Here we examine whether there is a possible relationship between DDL and the extended DMD (or EDMD) algorithm of Williams et al. [58]. For simplicity, we assume analyticity for the dynamical system ($r = a$) and hence we can write the inverse of the linearizing transformation (40) behind the DDL algorithm as a convergent Taylor expansion of the form

$$\gamma = \kappa^{-1}(\varphi) = \varphi + \sum_{|\mathbf{k}|=2}^{\infty} \mathbf{q}_{\mathbf{k}} \varphi^{\mathbf{k}}. \quad (42)$$

We then differentiate this equation in time to obtain from the linearized equation (38) a d -dimensional system of equations

$$\dot{\varphi} + \sum_{|\mathbf{k}|=2}^{\infty} \mathbf{q}_{\mathbf{k}} \frac{d}{dt} \varphi^{\mathbf{k}} = \mathbf{B} \varphi + \sum_{|\mathbf{k}|=2}^{\infty} \mathbf{B} \mathbf{q}_{\mathbf{k}} \varphi^{\mathbf{k}}$$

that the restricted observable φ and its monomials $\varphi^{\mathbf{k}}$ must satisfy. This last equation can be rewritten as a d -dimensional autonomous system of linear system of ODEs,

$$\begin{bmatrix} \mathbf{I}_{d \times d} & \mathbf{Q}_2 \end{bmatrix} \frac{d}{dt} \begin{bmatrix} \varphi \\ \mathbf{K}_{\geq 2}(\varphi) \end{bmatrix} = \begin{bmatrix} \mathbf{B} & \mathbf{B} \mathbf{Q}_2 \end{bmatrix} \begin{bmatrix} \varphi \\ \mathbf{K}_{\geq 2}(\varphi) \end{bmatrix}, \quad (43)$$

for the reduced observable φ and the infinite-dimensional vector $\mathbf{K}_{\geq 2}(\varphi)$ of all nonlinear monomials of φ . Here $\mathbf{I}_{d \times d}$ denotes the d -dimensional identity matrix and \mathbf{Q}_2 contains all coefficients \mathbf{q}_k as column vectors starting from order $|\mathbf{k}| = 2$.

If we truncate the infinite-dimensional vector of monomials $\mathbf{K}_{\geq 2}(\varphi)$ to the vector $\mathbf{K}_2^k(\varphi)$ of nonlinear monomials up to order k , then eq. (43) becomes

$$\begin{bmatrix} \mathbf{I}_{d \times d} & \mathbf{Q}_2^k \end{bmatrix} \frac{d}{dt} \begin{bmatrix} \varphi \\ \mathbf{K}_2^k(\varphi) \end{bmatrix} = \begin{bmatrix} \mathbf{B} & \mathbf{BQ}_2^k \end{bmatrix} \begin{bmatrix} \varphi \\ \mathbf{K}_2^k(\varphi) \end{bmatrix}. \quad (44)$$

This is a d -dimensional implicit system of linear ODEs for the dependent variable vector $(\varphi, \mathbf{K}_2^k(\varphi))$ whose dimension is always larger than d . Consequently, the operator $\begin{bmatrix} \mathbf{I}_{d \times d} & \mathbf{Q}_2^k \end{bmatrix}$ is never invertible and hence, contrary to the assumption of EDMD, there is no well-defined linear system of ODEs that governs the evolution of an observable vector and the monomials of its components.

The above conclusion remains unchanged even if one attempts to optimize with respect to the choice of the coefficients \mathbf{q}_k in the matrix \mathbf{Q}_2^k .

4.3 Implementation and applications of DDL

4.3.1 Basic implementation of DDL for model reduction and linearization

Theorem 4 allows us to define a numerical procedure to construct a linearizing transformation on the d -dimensional attracting slow manifold $\mathcal{W}(E)$ systematically from data. From eq. (44), the matrices \mathbf{B} and \mathbf{Q} are to be determined, given a set of observed trajectories. In line with the notation used in Section 4.2, let the data matrix $\mathbf{K}_2^k(\varphi)$ contain monomials (from order 2 to order k) of the observable vector φ and let $\hat{\mathbf{K}}_2^k(\varphi)$ contain denote the evaluation of $\mathbf{K}_2^k(\varphi)$ time Δt later. Passing to the discrete version of the invariance equation (44), we obtain

$$\begin{bmatrix} \mathbf{I} & \mathbf{Q} \end{bmatrix} \begin{bmatrix} \hat{\varphi} \\ \hat{\mathbf{K}}_2^k(\varphi) \end{bmatrix} = \begin{bmatrix} \mathbf{B} & \mathbf{BQ} \end{bmatrix} \begin{bmatrix} \varphi \\ \mathbf{K}_2^k(\varphi) \end{bmatrix}$$

for some matrices $\mathbf{Q} \in \mathbb{R}^{d \times N(d,k)-d}$ and $\mathbf{B} = e^{\mathbf{B}\Delta t} \in \mathbb{R}^{d \times d}$. Moreover, the inverse transformation of the linearization on the SSM $\mathcal{W}(E)$ is well-defined, and hence with an appropriate matrix $\mathbf{Q}^{inv} \in \mathbb{R}^{d \times N(d,k)-d}$, we can write

$$\begin{bmatrix} \mathbf{I} & \mathbf{Q}^{inv} \end{bmatrix} \begin{bmatrix} \varphi + \mathbf{QK}_2^k(\varphi) \\ \mathbf{K}_2^k(\varphi + \mathbf{QK}_2^k(\varphi)) \end{bmatrix} = \varphi.$$

This allows us to define the cost functions

$$\begin{aligned} \mathcal{L}^{(1)}(\mathbf{Q}, \mathbf{B}) &= \left| \begin{bmatrix} \mathbf{I} & \mathbf{Q} \end{bmatrix} \begin{bmatrix} \hat{\varphi} \\ \hat{\mathbf{K}}_2^k(\varphi) \end{bmatrix} - \begin{bmatrix} \mathbf{B} & \mathbf{BQ} \end{bmatrix} \begin{bmatrix} \varphi \\ \mathbf{K}_2^k(\varphi) \end{bmatrix} \right|^2, \\ \mathcal{L}^{(2)}(\mathbf{Q}, \mathbf{Q}^{inv}) &= \left| \mathbf{QK}_2^k(\varphi) + \mathbf{Q}^{inv} \mathbf{K}_2^k(\varphi + \mathbf{QK}_2^k(\varphi)) \right|^2, \end{aligned} \quad (45)$$

where $\mathcal{L}^{(1)}$ measures the invariance error along the observed trajectories and $\mathcal{L}^{(2)}$ measures the error due to the computation of the inverse. We aim to jointly minimize $\mathcal{L}^{(1)}$ and $\mathcal{L}^{(2)}$. To this end, we define the combined cost function

$$\mathcal{L}_\nu(\mathbf{Q}, \mathbf{Q}^{inv}, \mathbf{B}) = \mathcal{L}^{(1)}(\mathbf{Q}, \mathbf{B}) + \nu \mathcal{L}^{(2)}(\mathbf{Q}, \mathbf{Q}^{inv}), \quad (46)$$

for some $\nu \geq 0$. In our examples, we choose $\nu = 1$, which puts the same weight on both terms in the cost function (46). Minimizers of \mathcal{L}_ν provide optimal solutions to the DDL principle and can be written as

$$(\mathbf{Q}^*, \mathbf{Q}^{inv,*}, \mathbf{B}^*) = \underset{\mathbf{Q}, \mathbf{Q}^{inv}, \mathbf{B}}{\operatorname{argmin}} \mathcal{L}_\nu(\mathbf{Q}, \mathbf{Q}^{inv}, \mathbf{B}), \quad (47)$$

or, equivalently, as solutions of the system of equations

$$\frac{\partial \mathcal{L}_\nu}{\partial Q_{ij}} = 0 \quad i = 1, \dots, d, j = 1, \dots, N(d, k) - d, \quad (48)$$

$$\frac{\partial \mathcal{L}_\nu}{\partial Q_{ij}^{inv}} = 0, \quad i = 1, \dots, d, j = 1, \dots, N(d, k) - d, \quad (49)$$

$$\frac{\partial \mathcal{L}_\nu}{\partial \mathcal{B}_{ij}} = 0 \quad i, j = 1, \dots, d.$$

The optimal solution (47) does not necessarily coincide with the Taylor-coefficients of the linearizing transformation (41). Instead of giving the best local approximation, $(\mathbf{Q}^*, \mathbf{Q}^{inv,*}, \mathcal{B}^*)$ approximates the linearizing transformation and the linear dynamics in a least-squares sense over the domain of the training data. This means that DDL is not hindered by the convergence properties of the analytic linearization. Note that for $d = 1$, one can estimate the radius of convergence of (41), for example, by constructing the Domb-Skyes plot (see Domb and Sykes [15]), or by finding the radius of the circle in the complex plane onto which the roots of the truncated expansion accumulate under increasing orders of truncation (see Jentzsch [25], Ponsioen et al. [47]). For $d > 1$, such analysis is more difficult, since multivariate Taylor-series have more complicated domains of convergence. In our numerical examples, we estimate the domain of convergence of such analytic linearizations as the domain on which $\kappa \circ \kappa^{-1} = \mathbf{I}$ holds to a good approximation. As we will see, this domain of convergence may be substantially smaller than the domain of validity of transformations determined in a fully data-driven way.

Since the cost function (45) is not convex, the optimization problem (47) has to be solved iteratively starting from an initial guess $(\mathbf{Q}_0, \mathbf{Q}_0^{inv}, \mathcal{B}_0)$. For the examples presented in the paper, we use the Levenberg–Marquardt algorithm (see Bates and Watts [4]), but other nonlinear optimization methods, such as gradient descent or Adam (see Kingma and Ba [29]) could also be used. For our implementation, which is available from the repository Kaszás et al. [28], we used the Scipy and Pytorch libraries of Virtanen et al. [57], Paszke et al. [45]. In summary, we will use the following Algorithm 1 in our examples for model reduction via DDL.

Algorithm 1: Model reduction with DDL

Data:

d : Dimension of the slow SSM $\mathcal{W}(\mathcal{E})$.

k : Maximal polynomial order.

$\varphi, \hat{\varphi} \in \mathbb{R}^{d \times n_{samples}}$: Data matrices of the reduced coordinates and their forward-shifted images. The input data may need to be truncated, in order to ensure that it lies sufficiently close to the SSM. This needs to be checked, e.g., by time-frequency analysis (see Cenedese et al. [12]).

$\nu \geq 0$: Weight parameter in the cost function

tol : Tolerance value for the cost function.

Result:

$\mathbf{Q} \in \mathbb{R}^{d \times N(d,k)-d}$: Coefficients of the transformation $\varphi = \kappa(\gamma)$.

$\mathbf{Q}^{inv} \in \mathbb{R}^{d \times N(d,k)-d}$: Coefficients of the inverse transformation $\gamma = \kappa^{-1}(\varphi)$.

\mathcal{B} : The linear dynamics.

- 1 Compute the monomials $\mathbf{K}_2^k(\varphi), \hat{\mathbf{K}}_2^k(\varphi) \in \mathbb{R}^{N(d,k)-d \times n_{samples}}$
 - 2 Choose an initial guess, either randomly or inferred from DMD
 - 3 $(\mathbf{Q}, \mathbf{Q}^{inv}, \mathcal{B}) \leftarrow (\mathbf{Q}_0, \mathbf{Q}_0^{inv}, \mathcal{B}_0)$
 - 4 **while** $\mathcal{L}_\nu(\mathbf{Q}, \mathbf{Q}^{inv}, \mathcal{B}) > tol$ **do**
 - 5 Compute the monomials $\mathbf{K}_2^k(\varphi + \mathbf{Q}\mathbf{K}_2^k(\varphi))$
 - 6 Evaluate $\mathcal{L}_\nu(\mathbf{Q}, \mathbf{Q}^{inv}, \mathcal{B}) = \mathcal{L}^{(1)}(\mathbf{Q}, \mathcal{B}) + \nu\mathcal{L}^{(2)}(\mathbf{Q}, \mathbf{Q}^{inv})$
 - 7 Perform *Optimization step* (e.g., Levenberg–Marquardt or gradient descent)
 - 8 $(\mathbf{Q}, \mathbf{Q}^{inv}, \mathcal{B}) \leftarrow (\mathbf{Q}_{new}, \mathbf{Q}_{new}^{inv}, \mathcal{B}_{new})$
 - 9 **end**
-

Remark 3. The expressions (45)-(46) define one of the possible choices for the cost function. With $\nu = 0$, (46) simply corresponds to a one-step-ahead prediction with the linearized dynamics. Alternatively, a multi-step prediction can also be enforced. For a training trajectory $\varphi(t)$, the invariance

$$\begin{bmatrix} \mathbf{I} & \mathbf{Q} \end{bmatrix} \begin{bmatrix} \varphi \\ \mathbf{K}_2^k(\varphi) \end{bmatrix} = \begin{bmatrix} \mathcal{B}^{1:m} & \mathcal{B}^{1:m}\mathbf{Q} \end{bmatrix} \begin{bmatrix} \varphi(0) \\ \mathbf{K}_2^k(\varphi(0)) \end{bmatrix}$$

could be required, where $\mathcal{B}^{1:m}$ is a tensor composed of powers of the linear map \mathcal{B} . Optimizing over the entire trajectory is, however, more costly than simply minimizing (45), and we found no noticeable improvement in accuracy in our numerical examples.

4.3.2 Relationship with DMD implementations

Note that setting $\mathbf{Q} = \mathbf{Q}^{inv} = \mathbf{0}$ in the optimization problem (47) turns the problem into DMD. In this case, the usual DMD algorithm surveyed in the Introduction returns

$$\mathcal{B}_0 = \operatorname{argmin}_{\mathcal{B}} \mathcal{L}_0(\mathbf{0}, \mathbf{0}, \mathcal{B}),$$

which is a good initial guess for the non-convex optimization problem (47). More importantly, since Theorem 4 guarantees the existence of a near-identity linearizing transformation, we expect that the true minimizer is close to the DMD-solution. Therefore, we may explicitly expand the cost function

(45) around the DMD solution as

$$\begin{aligned} \mathcal{L}_\nu(\mathbf{Q}, \mathbf{Q}^{inv}, \mathcal{B}) &= \mathcal{L}_\nu(\mathbf{0}, \mathbf{0}, \mathcal{B}_0) + D\mathcal{L}_{(\mathbf{0}, \mathbf{0}, \mathcal{B}_0)} \cdot \begin{pmatrix} \mathbf{Q} \\ \mathbf{Q}^{inv} \\ \mathcal{B} - \mathcal{B}_0 \end{pmatrix} \\ &+ \frac{1}{2} \left[D^2\mathcal{L}_{(\mathbf{0}, \mathbf{0}, \mathcal{B}_0)} \cdot \begin{pmatrix} \mathbf{Q} \\ \mathbf{Q}^{inv} \\ \mathcal{B} - \mathcal{B}_0 \end{pmatrix} \right] \cdot \begin{pmatrix} \mathbf{Q} \\ \mathbf{Q}^{inv} \\ \mathcal{B} - \mathcal{B}_0 \end{pmatrix} \\ &+ (|\mathbf{Q}|^3, |\mathbf{Q}^{inv}|^3, |\mathcal{B} - \mathcal{B}_0|^3), \end{aligned}$$

where $D\mathcal{L}_{(\mathbf{0}, \mathbf{0}, \mathcal{B}_0)}$ and $D^2\mathcal{L}_{(\mathbf{0}, \mathbf{0}, \mathcal{B}_0)}$ are the Jacobian and the Hessian of the cost function evaluated at the DMD solution, respectively. Since the Jacobian is nonsingular at the DMD solution, the minimum of the quadratic approximation of the cost function satisfies the linear equation

$$-D\mathcal{L}_{(\mathbf{0}, \mathbf{0}, \mathcal{B}_0)} = D^2\mathcal{L}_{(\mathbf{0}, \mathbf{0}, \mathcal{B}_0)} \begin{pmatrix} \mathbf{Q} \\ \mathbf{Q}^{inv} \\ \mathcal{B} - \mathcal{B}_0 \end{pmatrix}. \quad (50)$$

This serves as the first-order correction to the DMD-solution in the DDL procedure. The equation (50) is explicitly solvable and is equivalent to performing a single Levenberg–Marquardt step on the non-convex cost function (45), with the DMD solution $(\mathbf{0}, \mathbf{0}, \mathcal{B}_0)$ serving as an initial guess.

Minimization of (45) leads to a non-convex optimization problem. Besides computing the leading-order approximation (50), a possible workaround to this challenge is to carry out the linearization in two steps. First, one can fit a polynomial map to the reduced dynamics by linear regression. Then, if the reduced-dynamics is non-resonant, it can be analytically linearized. Ax&as et al. [3] follow this approach to automatically find the extended normal form style reduced dynamics on SSMs using the implementation of SSMTTool by Jain et al. [24]. Although this procedure does convert the DDL principle into a convex problem, the drawback is that the linearization is obtained as a Taylor-expansion, with possibly limited convergence properties.

4.3.3 Using DDL to construct spectral foliations

The mathematical foundation of SSM-reduced modeling is that any trajectory converging to a slow SSM is guaranteed to synchronize up to an exponentially decaying error with one of the trajectories on the SSM. This follows from the general theory of invariant foliations by Fenichel [18], when applied to the d -dimensional normally hyperbolic invariant manifold $\mathcal{W}(E)$.² The main result of the theory is that off-SSM initial conditions synchronizing with the same on-SSM trajectory turn out to form a class C^{r-1} smooth, $(n-d)$ -dimensional manifold, denoted $\mathcal{F}_{\mathbf{p}}$, which intersects $\mathcal{W}(E)$ in a unique point $\mathbf{p} \in \mathcal{W}(E)$. The manifold $\mathcal{F}_{\mathbf{p}}$ is called the stable fiber emanating from the base point \mathbf{p} . Fenichel proves that any off-SSM trajectory $\mathbf{x}(t; \mathbf{x}_0)$ with initial condition $\mathbf{x}_0 \in \mathcal{F}_{\mathbf{p}_0}$ converges to the specific on-SSM trajectory $\mathbf{p}(t; \mathbf{p}_0) \in \mathcal{W}(E)$ with initial condition $\mathbf{p}_0 \in \mathcal{W}(E)$ faster than any other nearby trajectory might converge to $\mathbf{p}(t; \mathbf{p}_0)$. Recently, Szalai [55] studied this foliation in more detail under the name “invariant spectral foliation”, discussed its uniqueness in an appropriate smoothness class and proposed its use in model reduction.

To predict the evolution of a specific, off-SSM initial condition \mathbf{x}_0 up to time t from an SSM-based model, we first need to relate that initial condition to the base point \mathbf{p}_0 of the stable fiber $\mathcal{F}_{\mathbf{p}_0}$. Next, we need to run the SSM-based reduced model up to time t to obtain $\mathbf{p}(t; \mathbf{p}_0)$. Based on the exponentially fast convergence of the full solution $\mathbf{x}(t; \mathbf{x}_0)$ to the SSM-reduced solution $\mathbf{p}(t; \mathbf{p}_0)$, we obtain an accurate longer-term prediction for $\mathbf{x}(t; \mathbf{x}_0)$ using this procedure. Such a longer-term

²More precisely, Fenichel’s foliation results become applicable after the wormhole construct in Proposition B1 of Eldering et al. [17] is applied to extend $\mathcal{W}(E)$ smoothly into a compact normally attracting invariant manifold without boundary. This is needed because Fenichel’s results only apply to compact normally attracting invariant manifolds with an empty or overflowing boundary, whereas the boundary of $\mathcal{W}(E)$ is originally inflowing.

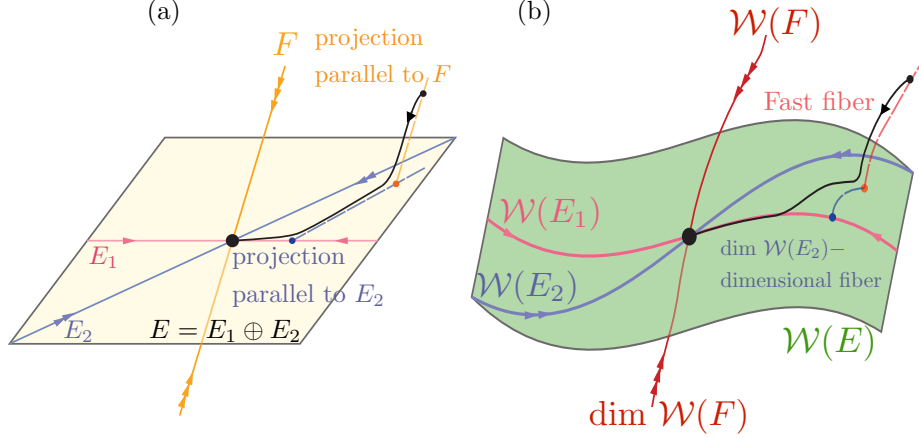


Figure 2: (a): The linearized phase space geometry governed by the slow spectral subspace $E = E_1 \oplus E_2$ and the slow invariant foliation within E . (b): Phase space geometry in the original coordinates.

prediction is helpful, for instance, when we wish to predict steady states, such as fixed points and limit cycles, from the SSM-reduced dynamics.

Constructing this spectral foliation directly from data, however, is challenging for nonlinear systems. Indeed, one would need a very large number of initial conditions that cover uniformly a whole open neighborhood of the fixed point in the phase space. For example, while one or two training trajectories are generally sufficient to infer accurate SSM-reduced models even for very high-dimensional systems (see e.g., Cenedese et al. [12, 13], Axâs et al. [3]), thousands of uniformly distributed initial conditions in a whole open set of a fixed point are required to infer accurate spectral foliation-based models even for low-dimensional systems (see Szalai [55]). The latter number and distribution of initial conditions is unrealistic to acquire in a truly data-driven setting.

To avoid constructing the full foliation, one may simply project an initial condition x_0 orthogonally to an observed spectral submanifold $\mathcal{W}(E)$ to obtain \mathbf{p}_0 , but this may result in large errors if E and F are not orthogonal. In that case, $\mathcal{W}(E)$ may divert substantially from E (see [48, 42, 43] for a discussion of the limitations of this projection for general invariant manifolds).

A better solution is to project \mathbf{x}_0 orthogonally to the slow spectral subspace E over which $\mathcal{W}(E)$ is a graph in an (often large) neighborhood of the fixed point. This approach assumes that E and F are nearly normal and $\mathcal{W}(E)$ is nearly flat. As the latter is typically the case for delay-embedded observables (Axâs and Haller [2]), orthogonal projection onto E has been the choice so far in data-driven SSM-based reduction via the SSMLearn algorithm (Cenedese et al. [11]). This approach has produced highly accurate reduced-order models in a number of examples (see Cenedese et al. [12, 13], Axâs et al. [3]). There are nevertheless examples in which the linear part of the dynamical system is significantly non-normal and hence E and F are not close to being orthogonal (see Bettini et al. [6]).

Near hyperbolic fixed points, the use of DDL eliminates the need to construct involved nonlinear spectral foliations. Indeed, let us assume that the slow spectral subspace E in Theorem 4 can be decomposed into a direct sum $E = E_1 \oplus E_2$, where E_1 denotes the slowest spectral subspace with $\dim E_1 = d_1$ and E_2 denotes the second-slowest spectral subspace with $\dim E_2 = d_2$, as sketched in Fig. 2. Reducing the dynamics to the SSM $\mathcal{W}(E)$ is accurate for transient times given by the decay rate of E_2 . This initial reduction can be done simply by a normal projection onto E . Inside E , one can simply locate spectral foliations of the DDL-linearized systems explicitly and map them back to the original nonlinear system under the DDL transformation $\kappa(\gamma)$. The unique class C^a foliation

of a linear system within E is the family of stable fibers forming the affine space

$$\mathcal{F}_{\mathbf{p}} = \mathbf{p} + E_2,$$

where $\mathbf{p} \in E_1$. The trajectories started inside $\mathcal{F}_{\mathbf{p}}$ all synchronize with $\mathbf{p} \in E_1$. The linear projection \mathbf{P}_{E_2} onto E_1 along directions parallel to E_2 , when applied to an initial condition $\mathbf{y} \in \mathcal{F}_{\mathbf{p}}$, returns the base point

$$\mathbf{P}_{E_2}\mathbf{y} = \mathbf{p}. \quad (51)$$

In the nonlinear system (1), the leaves of the smooth foliation within $\mathcal{W}(E)$

$$\mathcal{F}_{\kappa(\mathbf{p})}^0 = \kappa(\mathcal{F}_{\mathbf{p}}) \subset \mathcal{W}(E),$$

where $\kappa(\mathbf{p}) \in \mathcal{W}(E_1)$ is the image of \mathbf{p} under the mapping κ defined in (37). The SSM $\mathcal{W}(E)$ can then be parametrized via the foliation

$$\mathcal{W}(E) = \bigcup_{\mathbf{q} \in \mathcal{W}(E_1)} \mathcal{F}_{\mathbf{q}}^0.$$

4.3.4 Using DDL to predict nonlinear forced response from unforced data

We now discuss how DDL performed near the fixed point of an autonomous dynamical system can be used to predict nonlinear forced response under additional weak periodic forcing in the domain of DDL. The addition of such small forcing is frequent in structural vibration problems in which the unforced structure (e.g., a beam or disk) is rigid enough to react with small displacements under practically relevant excitation levels (see, e.g., Cenedese et al. [12, 13] for specific examples).

We append system (11) with a small, time-periodic forcing term $\varepsilon \mathbf{F}(\mathbf{x}, t)$ to obtain the system

$$\dot{\mathbf{x}} = \mathbf{A}\mathbf{x} + \tilde{\mathbf{f}}(\mathbf{x}) + \varepsilon \mathbf{F}(\mathbf{x}, t), \quad \mathbf{x} \in \mathbb{R}^n, \quad \mathbf{A} = D\mathbf{f}(0), \quad \tilde{\mathbf{f}}(\mathbf{x}) = \mathcal{O}(|\mathbf{x}|^2), \quad 0 \leq \varepsilon \ll 1, \quad (52)$$

with $\mathbf{F}(\mathbf{x}, t) = \mathbf{F}(\mathbf{x}, t + T)$ for some period $T > 0$. If the conditions of Theorem 4 hold for the system (52) for $\varepsilon = 0$, then, for $\varepsilon > 0$ small enough, exists a unique d -dimensional, T -periodic, attracting spectral submanifold $\mathcal{W}_\varepsilon(E, t) \in C^r$ of a locally unique attracting T -periodic orbit $\mathbf{x}_\varepsilon(t)$ perturbing from $\mathbf{x} = \mathbf{0}$ (see, e.g., Cabré et al. [10], Haller and Ponsioen [21]). The manifold $\mathcal{W}_\varepsilon(E, t)$ is $\mathcal{O}(\varepsilon)$ C^1 -close to $\mathcal{W}_0(E, t) \equiv \mathcal{W}(E)$ and hence its reduced dynamics can be parametrized using the reduced observable vector $\varphi = \phi|_{\mathcal{W}(E)}$ in the form

$$\begin{aligned} \dot{\varphi} &= \mathbf{B}\varphi + \mathbf{q}(\varphi) + \varepsilon \hat{\mathbf{F}}(\varphi, t), \quad \mathbf{B} = D\phi(\mathbf{0})\mathbf{T}_E \Lambda_E (D\phi(\mathbf{0})\mathbf{T}_E)^{-1}, \quad \mathbf{q}(\varphi) = \mathcal{O}(|\varphi|^2), \quad (53) \\ \hat{\mathbf{F}}(\varphi, t) &= (D\phi(\mathbf{0})\mathbf{T}_E)^{-1} (\mathbf{I} + D\mathbf{h}(\varphi, \mathbf{0}))^{-1} \mathbf{F}(\mathbf{0}, t) + \mathcal{O}(\varepsilon |\varphi|^2), \end{aligned}$$

where we have relegated the details of this calculation to Appendix E.

Then the unique, C^r change of coordinates,

$$\varphi = \kappa(\gamma) = \gamma + \ell(\gamma), \quad (54)$$

guaranteed by statement (iii) of Theorem 4 transforms the reduced dynamics (53) to its final form

$$\dot{\gamma} = \mathbf{B}\gamma + \varepsilon (\mathbf{I} + D\ell(\gamma))^{-1} \hat{\mathbf{F}}(\mathbf{0}, t). \quad (55)$$

The transformation is valid on trajectories of (52) as long as they remain in the domain of definition of the coordinate change (54).

Note that eq. (55) is a weakly perturbed, time-periodic nonlinear system. The matrix \mathbf{B} and the nonlinear terms $\ell(\gamma)$ can be determined using data from the unforced ($\varepsilon = 0$) system. As a result, nonlinear time-periodic forced response can be predicted *solely from unforced data* by applying

numerical continuation to system (55) for $\varepsilon > 0$. This is not expected to be as accurate as SSM-based forced response prediction (see, e.g., Cenedese et al. [12, 13], Axâs et al. [3], Axâs and Haller [2]), but nevertheless offers a way to make predictions for non-linearizable forced response based solely on DDL performed on unforced data. These predictions are valid for forced trajectories that stay in the domain of convergence of DDL carried out on the unforced system. We will illustrate such predictions using actual experimental data from fluid sloshing in Section 5.4.

Setting $\ell(\gamma) = 0$ in formula (55) enables us to carry out a forced-response prediction based on DMD as well. Such a prediction will be fundamentally linear with respect to the forcing and can only be reasonably accurate for very small forcing amplitudes, as we will indeed see in examples. There is no systematic way to model the addition of non-autonomous forcing in the EDMD procedure, and hence EDMD will not be included in our forced response prediction comparisons.

We also note, that one might be tempted to solve an approximate version of (55) by assuming

$$\varepsilon(\mathbf{I} + D\ell(\gamma))^{-1} \approx \varepsilon\mathbf{I}. \quad (56)$$

This assumption simplifies the computation of the forced response of the nonlinear system (55) to those of a simple linear system. Although the forced response computed using this approximate DDL method turns out to be more accurate than DMD on our example, we do not recommend this approach. This is because neglecting the nonlinear effects of the coordinate change in (55) is, in general, inconsistent with $\ell(\gamma) \neq 0$. We give more detail on this approximation in Appendix F of the Supplementary Information.

5 Examples

In this section, we compare the DMD, EDMD and DDL algorithms on specific examples. When applicable, we also compute the exact analytic linearization of the dynamical system near its fixed point as a benchmark. On a slow SSM $\mathcal{W}(E)$, an observer trajectory $\varphi(t)$, starting from a select initial condition $\varphi(0)$, will be tracked as the image of the linearized reduced observer trajectory $\gamma(t)$ under the linearizing transformation (54):

$$\varphi(t) = \kappa(e^{\mathbf{B}t}\gamma(0)) = e^{\mathbf{B}t}\gamma(0) + \ell(e^{\mathbf{B}t}\gamma(0)), \quad \gamma(0) = \kappa^{-1}(\varphi(0)). \quad (57)$$

When model reduction has also taken place, i.e., when the observable vector φ is not defined on the full phase space, we will nevertheless provide a prediction in the full phase space via the parametrization of the slow SSM.

By Theorem 1, DMD can be interpreted as setting $\ell(\gamma) \equiv 0$ in (57) and finding the linear operator \mathbf{B} as a best fit from the available data. In contrast, DDL finds the linear operator \mathbf{B} , the transformation $\varphi = \gamma + \ell(\gamma)$, and its inverse simultaneously. As we explained in Section 4.2, EDMD cannot quite be interpreted in terms of the linearizing transformation (57) as it is an attempt to immerse the dynamics into a higher dimensional space. For our EDMD tests, we will use monomials of the observable vector φ .

5.1 1D nonlinear system with two isolated fixed points

Consider the one-dimensional ODE obtained as the radial component of the Stuart-Landau equation, i.e.,

$$\dot{r} = \mu r - r^3,$$

which can be rescaled to

$$\dot{R} = R - R^3. \quad (58)$$

For $R \geq 0$, the system has a repelling fixed point at $R = 0$ and an attracting one at $R = 1$. Page and Kerswell [44] show that local expansion of observables in terms of the Koopman eigenfunctions computed near each fixed point are possible, but the expansions at the two fixed points are not

compatible with each other and both diverge at $R = \sqrt{2}/2$. This is a consequence of the more general result that the Koopman eigenfunctions themselves typically blow up near basin boundaries (see our Proposition 1 in Appendix A of the Supplementary Information). Both DMD and EDMD can nevertheless be computed from data, even for a trajectory crossing the turning point at $R = \sqrt{2}/2$, but the resulting models cannot have any connection to the Koopman operator.

In each comparison performed on system (58), we generate a single trajectory in the domain of attraction of the $R = 1$ fixed point and use it as training data for DMD, EDMD and DDL. In each subplot of Fig. 3, the single training trajectory starts from the intersection of the red horizontal line “IC of training trajectory” with the $t = 0$ dashed line. We then also generate a new test trajectory (black) with its initial condition denoted with a black dot over the line $t = 0$. We place this initial condition slightly outside the domain of linearization for system (58) (under the grey line labeled “Turning point”). We use DMD, order- $k = 5$ EDMD, and DDL trained on a single training trajectory to make predictions for the black testing trajectory (not used in the training).

Figure 3a shows DDL to be the most accurate of the three methods when applied to forward-time ($t \geq 0$) segments of the test trajectory. If we try to predict the backward-time ($t < 0$) segment of the same trajectory as it leaves the training domain, DDL diverges immediately upwards, whereas DMD and EDMD diverge more gradually downwards. As we increase the training domain in Fig 3b, DDL continues to be the most accurate in both forward and backward time until it reaches the domain of its training range in backward time. At that point, it diverges quickly upwards, while DMD and EDMD diverge more slowly downwards.

Importantly, increasing the approximation order for DDL first to $k = 10$ then to $k = 18$ (see Figs. 3c-d), makes DDL predictions more and more accurate in backward time inside the training domain. At the same time, the same increase in order makes EDMD less and less accurate inside the same domain. This is not surprising for EDMD because it seeks to approximate the dynamics within a Koopman-invariant subspaces for increasing k , and Koopman mode expansions blow up at the “Turning point line”, as shown both analytically and numerically by Page and Kerswell [44]. Interestingly, however, EDMD becomes less accurate even within the domain of linearization under increasing k . This is clearly visible in Fig. 3d which shows spurious, growing oscillations in the EDMD predictions close to the $R = 1$ fixed point.

In summary, of the three methods tested, DDL makes the most accurate predictions in forward time. This remains true in backward time as long as the trajectory remains in the training range used for the three methods, even if this range is larger than the theoretical domain of linearization. Inside the training range, an increase of the order k of the monomials used increases the accuracy of DDL but introduces growing errors in EDMD.

5.2 3D linear system studied via nonlinear observables

Wu et al. [60] studied the ability of DMD to recover a 3D linear system based on the time history of three nonlinear observables evaluated on the trajectories of the system. To define the linear system, they use a block-diagonal matrix $\mathbf{\Lambda}$ and a basis transformation matrix \mathbf{R} of the form

$$\mathbf{\Lambda} = \begin{pmatrix} a & -b & 0 \\ b & a & 0 \\ 0 & 0 & c \end{pmatrix}, \quad a, b, c \in \mathbb{R}, \quad \mathbf{R} = \begin{pmatrix} 1 & 0 & \sin \theta_1 \cos \theta_2 \\ 0 & 1 & \sin \theta_1 \sin \theta_2 \\ 0 & 0 & \cos \theta_2 \end{pmatrix}, \quad (59)$$

to define the linear discrete dynamical system

$$\mathbf{x}(n+1) = (\mathbf{R}\mathbf{\Lambda}\mathbf{R}^{-1}) \mathbf{x}(n). \quad (60)$$

The linear change of coordinates \mathbf{R} rotates the real eigenspace of $\mathbf{\Lambda}$ corresponding to the eigenvalue c and hence introduces non-normality in system (60). This system is then assumed to be observed via a 3D nonlinear observable vector

$$\mathbf{y}(\mathbf{x}) = \begin{pmatrix} x_1 + 0.1(x_1^2 + x_2x_3) \\ x_2 + 0.1(x_2^2 + x_1x_3) \\ x_3 + 0.1(x_3^2 + x_1x_2) \end{pmatrix}. \quad (61)$$

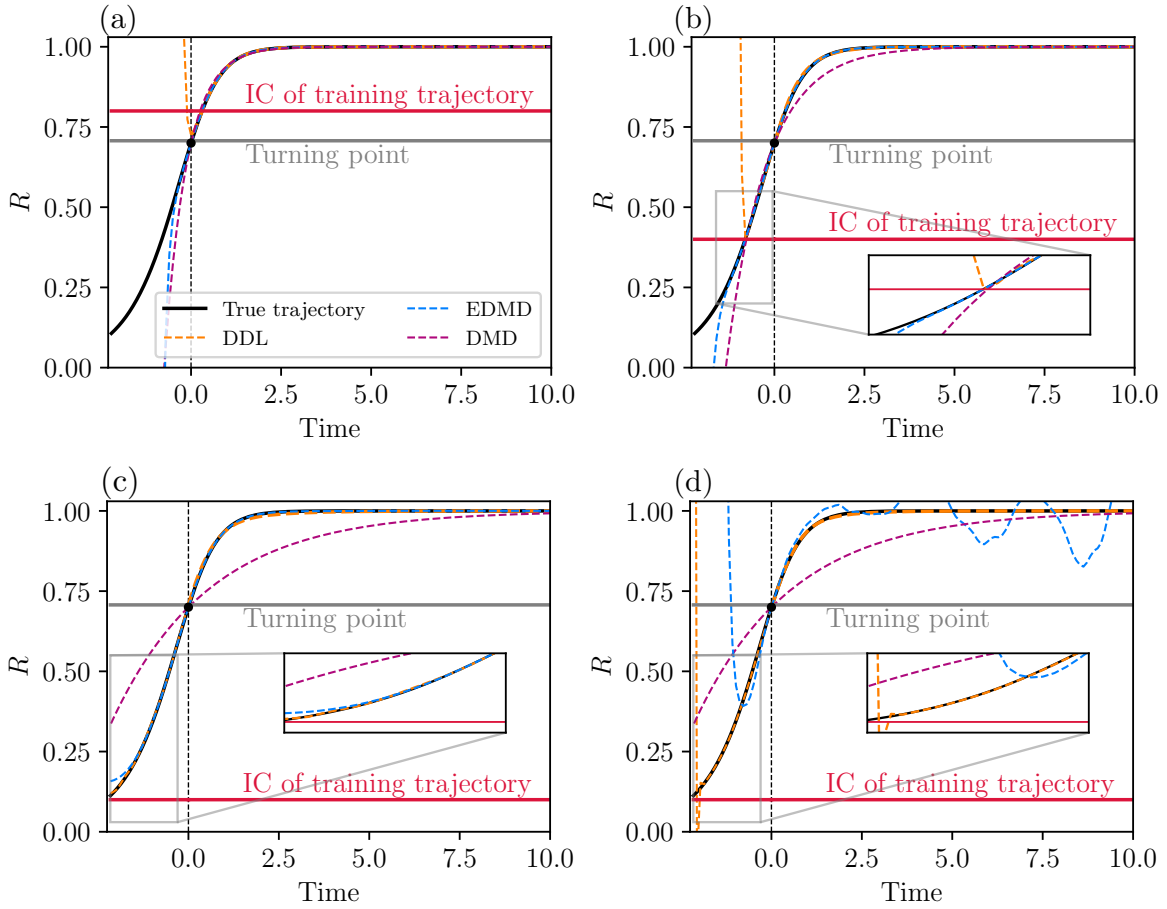


Figure 3: Predictions of DMD, EDMD and DDL on trajectories of (58). (a) Training trajectory starts inside the domain of convergence of the linearization, i.e. $R(0) = 0.8$ (see Page and Kerswell [44]). For both DDL and EDMD the order of the monomials used is $k = 5$. (b) Same for a different training trajectory with $R(0) = 0.4$ and $k = 5$ (c) Same for $R(0) = 0.1$ and $k = 10$ (d) Same for $R(0) = 0.1$ and $k = 18$.

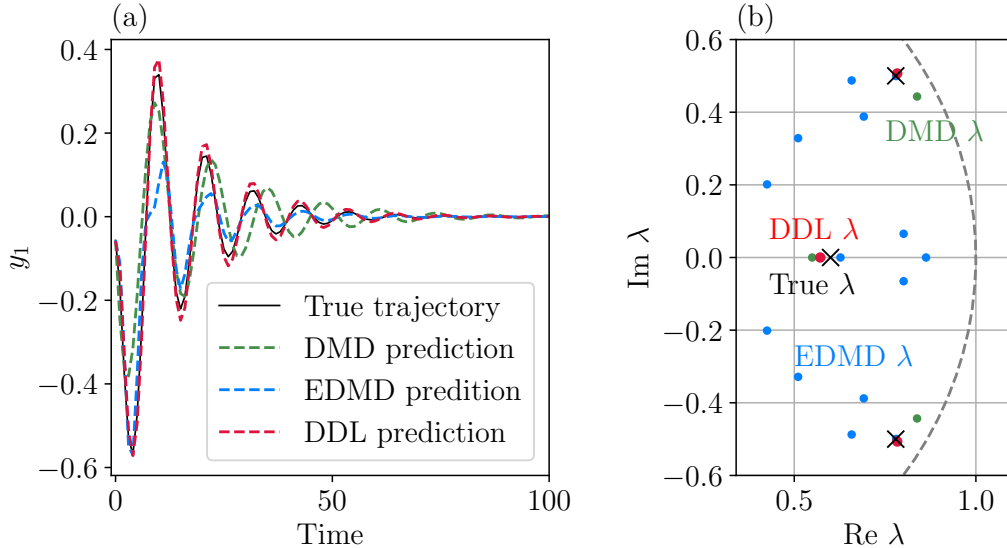


Figure 4: Predictions by DMD, EDMD, and DDL on the discrete dynamical system (59),(61).(a) Predicted and true y_1 -components of a test trajectory. (b) Spectra identified by DMD, EDMD, and DDL superimposed on the true spectrum (marked by crosses). The dashed line represents the unit circle.

Ideally, DMD should closely approximate the linear dynamics of system (60) because the observable function defined in eq. (61) is close to the identity and has only weak nonlinearities. Wu et al. [60] find, however, that this system poses a challenge for DMD, which produced inaccurate predictions for the spectrum of $\mathbf{R}\mathbf{A}\mathbf{R}^{-1}$.

Following one of the parameter settings of Wu et al. [60], we set $a = 0.45\sqrt{3}$, $b = 0.5$, $c = 0.6$, $\theta_1 = 1.5$, and $\theta_2 = 0$. We initialize three training trajectories with $\|\mathbf{x}(0)\| < 1$, each containing 100 iterations of system (60). We then compute the predictions of a 5th order DDL model and compare to those of DMD and EDMD on a separate test trajectory not used in training these three methods. The predictions and the spectrum obtained from the three methods are shown in Fig. 4.

The predictions of DMD and EDMD can only be considered accurate for very low amplitude oscillations, while DDL returns accurate predictions throughout the whole trajectory. This example consists of linear dynamics and monomial observables of the state, and hence should be an ideal test case for EDMD. Yet, EDMD is inaccurate in identifying the spectrum of system (60). Indeed, as seen in Fig. 4b, a number of spurious eigenvalues arise from EDMD, both real and complex. DMD performs clearly better but it is still markedly less accurate than DDL. These inaccuracies in the predictions of EDMD and DMD spectra are also reflected by considerable errors in their predictions for trajectories, as seen in Fig. 4a. In contrast, DDL produces the most accurate prediction for the test trajectory.

5.3 Damped and periodically forced Duffing equation

We consider the damped and forced Duffing equation

$$\begin{aligned} \dot{x} &= y, \\ \dot{y} &= x - x^3 - dy + \varepsilon \cos \Omega t, \end{aligned} \tag{62}$$

with damping coefficient $d = 0.0141$, forcing frequency Ω and forcing amplitude ε . We perform a change of coordinates $(x, y) \mapsto \varphi = (\varphi_1, \varphi_2)$ that moves the stable focus at $(x, y) = (1, 0)$ to the

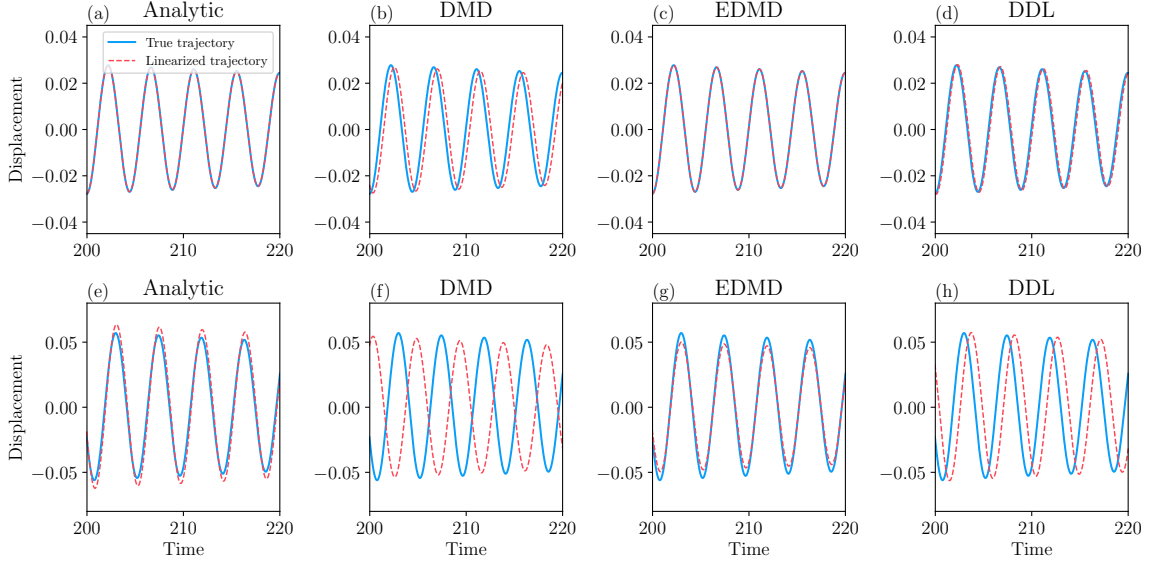


Figure 5: Comparison of the time evolution of the linearized trajectories (red) and the full trajectories of the nonlinear system (63) (blue), (63). (a)-(d): Analytic linearization, DMD, EDMD and DDL models trained and evaluated on trajectories inside the domain of convergence. (e)-(h): Same as (a)-(d) but outside the domain of convergence of the analytic linearization.

origin and makes the linear part block-diagonal. The resulting system is of the form

$$\dot{\varphi} = \mathbf{A}\varphi + \mathbf{f}(\varphi) + \varepsilon\hat{\mathbf{F}}(t), \quad \mathbf{f}(\varphi) = \mathcal{O}(|\varphi|^2), \quad (63)$$

where

$$\mathbf{A} = \begin{pmatrix} -\alpha & -\omega \\ \omega & -\alpha \end{pmatrix}, \quad \omega = 1.4142, \quad \alpha = 0.00707, \quad (64)$$

and $\hat{\mathbf{F}}(t)$ is the transformed image of the physical forcing vector in (62). We first consider the unforced system with $\varepsilon = 0$. In this case, the 2D slow SSM of the fixed point coincides with the phase space \mathbb{R}^2 and hence no further model reduction is possible. However, since the non-resonance conditions (34) hold for the linear part (64), the system is analytically linearizable near the origin. The linearizing transformation and its inverse can both be computed from eq. (63), as outlined in eq. (41). For reference, we carry out this linearization analytically up to order $k = 9$. The Taylor series of the linearization is estimated to converge for $|\varphi| < R_{crit} \approx 0.15$. The details of the calculation can be found in the repository [28].

We now compare the analytic linearization results it to DMD, EDMD and DDL, with all three trained on the same three trajectories, launched both inside and outside the domain of convergence of the analytic linearization. The polynomial order of approximation is $k = 5$ for both the EDMD and the DDL algorithms. The performance of the various methods is compared in Fig. 5. Close to the fixed point, in the domain of convergence of the analytic linearization, all three methods perform well. Moving away from the fixed point, the analytic linearization is no longer possible. Both DMD and EDMD perform worse, while DDL continues to accurately linearize the system even outside the domain of convergence of the analytic linearization.

Using formula (55) and our DDL-based model, we can also predict the response of system (63) for the forcing term of the form

$$\varepsilon\hat{\mathbf{F}}(t) = \varepsilon \begin{pmatrix} -0.006 \\ 1.225 \end{pmatrix} \cos \Omega t, \quad (65)$$

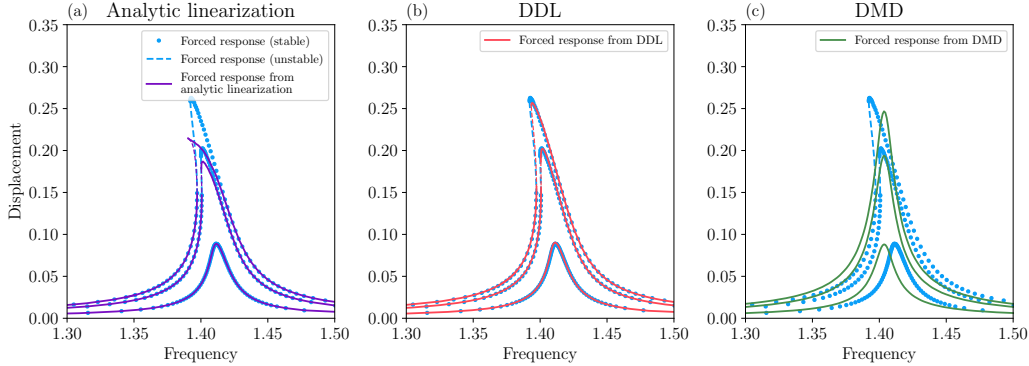


Figure 6: Periodic response of the Duffing oscillator under the forcing (63). The three distinctly colored forced response curves correspond to $\varepsilon = 0.001, 0.002, 0.0028$. (a) Actual nonlinear forced response from numerical continuation (blue) and prediction for it from analytic linearization (purple) (b) Forced response predictions from DDL (red) (c) Forced response predictions from DMD (green). The training data for panels (b) and (c) is the same unforced trajectory data set as the one used in Fig. 5.

without using any data from the forced system. As the forced DDL model (55) is nonlinear, it can capture non-linearizable phenomena such as coexisting of stable and unstable periodic orbits arising under the forcing. We can also make a forced response prediction from DMD simply by setting $D\ell(\gamma) = \mathbf{0}$ in eq. (55). As an inhomogeneous linear system of ODEs, however, this forced DMD model cannot predict coexisting stable and unstable periodic orbits.

In Fig. 6, we compare the forced predictions of the analytic linearization, DMD, and DDL to those computed from the nonlinear system directly via the continuation software COCO of Dankowicz and Schilder [14]. Since the forced and linearized systems are also nonlinear, we use the same continuation software to determine the stable and unstable branches of periodic orbits.

As expected, the analytic linearization is accurate while the forced response is inside the domain of convergence but deteriorates quickly for larger amplitudes. DMD gives good predictions for the peaks of the forced response diagrams, but cannot account for any of the nonlinear softening behavior, i.e., the overhangs in the curves that signal multiple coexisting periodic responses at the same forcing frequency. In contrast, while the DDL model of order $k = 5$ starts becoming inaccurate for peak prediction at larger amplitudes outside the domain of analytic linearization, it continues to capture accurately the overhangs arising from non-linearizable forced response away from the peaks. Notably, DDL even identifies the unstable branches (in dashed lines) of the periodic response accurately. For completeness, we also show results of approximate DDL, by assuming (56) in Appendix F.

5.4 Water sloshing experiment in a tank

In this section, we analyze experimental data generated by Bäuerlein and Avila [5] for forced and unforced fluid sloshing in a tank. Previous studies of this data set used nonlinear SSM-reduction to predict forced response (Cenedese et al. [12], Axås et al. [3], Axås and Haller [2]). Here we will use DMD and DDL to extract and compare linear reduced-order models from unforced trajectory data, then use them to predict and verify forced response curves obtained from forced trajectory data. Neither DMD nor DDL is expected to outperform the fully nonlinear approach of SSM reduction, so we will only compare them against each other.

The tank in the experiments is mounted on a platform that is displaced sinusoidally in time with various forcing amplitudes and frequencies (Fig. 7(a)). To train DMD and DDL, we use unforced sloshing data obtained by freezing the movement of the tank near a resonance and recording the

ensuing decaying oscillations of the water surface with a camera under they die out. The resulting videos serve as input data to our analysis. Specifically, the horizontal position of the center of mass of the fluid is extracted from each video frame tracked and used as the single scalar observable.

During such a resonance decay experiment, the system approaches its stable unforced equilibrium via oscillations that are dominated by a single mode. In terms of the phase space geometry, this means an approach to a stable fixed point along its 2D slow SSM $\mathcal{W}(E)$ tangent to the slowest 2D real eigenspace E . As we only have a single observable from the videos, we use delay embedding to generate a larger observable space that can accommodate the 2D manifold $\mathcal{W}(E)$. As discussed by Cenedese et al. [12], we need an at least 5D observable space for this purpose by the Takens embedding theorem. In this space, $\mathcal{W}(E)$ turns out to be nearly flat for short delays (see Ax as and Haller [2]), which allows us to use a linear approximation for its parametrization. The reduced coordinates on $\mathcal{W}(E) \approx E$ can then be identified via a singular value decomposition of the data after one removes initial transients from the experimental data. The end of the transients can be identified as a point beyond which a frequency analysis of the data shows only one dominant frequency, the imaginary part of the eigenvalue corresponding to E .

All this analysis has been carried out using the publicly available SSMLearn package Cenedese et al. [11]. With $\mathcal{W}(E)$ identified, we use the DDL method with order $k = 5$ to find the linearizing transformation and the linearized dynamics on $\mathcal{W}(E)$. In Fig 7(b) we show the prediction of the model on a decaying trajectory reserved for testing. The displacements are reported as percentage values, with respect to the depth of the tank. In Fig. 7c-d, we show predictions from the DMD and DDL models for the forced response, compared with the experimentally observed response. Since the exact forcing function is unknown, we follow the calibration procedure outlined by Cenedese et al. [12] to find an equivalent forcing amplitude in the reduced-order model.

We present data for three forcing amplitudes. The DDL predictions are accurate up to 0.17% amplitude, even capturing the softening trend. The largest-amplitude forcing resulted in response significantly outside the range of the training data; in this range, we were unable to find the converged forced response from DDL. We also show the corresponding DMD-predictions in Fig. 7c. Although the linear response can formally be evaluated for any forcing amplitude, DMD shows no trace of the softening trend, and is even inaccurate for low forcing amplitudes.

5.5 Model reduction and foliation in a nonlinear oscillator chain

As a final example, we consider the dynamics of a chain of nonlinear oscillators, which has been analyzed in the SSMLearn package Cenedese et al. [11]. Denoting the positions of the oscillators as q_i for $i = 1, \dots, 5$, we assume that the springs and dampers are linear, except for the first oscillator. The non-dimensionalized equations of motion can be written as

$$\mathbf{M}\ddot{\mathbf{q}} + \mathbf{C}\dot{\mathbf{q}} + \mathbf{K}\mathbf{q} + \mathbf{f}(\mathbf{q}, \dot{\mathbf{q}}) = \mathbf{0}, \tag{66}$$

where $\mathbf{M} = \mathbf{I}$; the springs have the same linear stiffness $k = 1$ which is encoded in \mathbf{K} via nearest-neighbor coupling. The damping is assumed to be proportional, i.e., we specifically set $\mathbf{C} = 0.002\mathbf{M} + 0.005\mathbf{K}$.

Three numerically generated training trajectories show decay to the $\mathbf{q} = \mathbf{0}$ fixed point, as expected from the damped nature of the linear part of the system. In this example, we also seek to capture some of the transients, which motivates us to select the slow SSM $\mathcal{W}(E)$ to be 4D, tangent to the spectral subspace $E = E_1 \oplus E_2$ spanned by the the slowest mode (E_1) and the second slowest mode (E_2). As the mode corresponding to E_2 does disappear over time from the decaying signal, there is no resonance between the eigenvalues and hence Theorem 4 is applicable. As already noted, numerical data from a generic physical system described by eq. (66) will be free from resonances. An exception is a 1: 1 resonance arising from a perfect symmetry, but this resonance is not excluded by Theorem 4 and has is amenable to DDL.

Within the 4D SSM $\mathcal{W}(E)$, we also demonstrate how to optimally reduce the dynamics to its 2D slowest SSM $\mathcal{W}(E_1)$. As explained in Section 4.3.3, to find the trajectory in $\mathcal{W}(E_1)$ with which

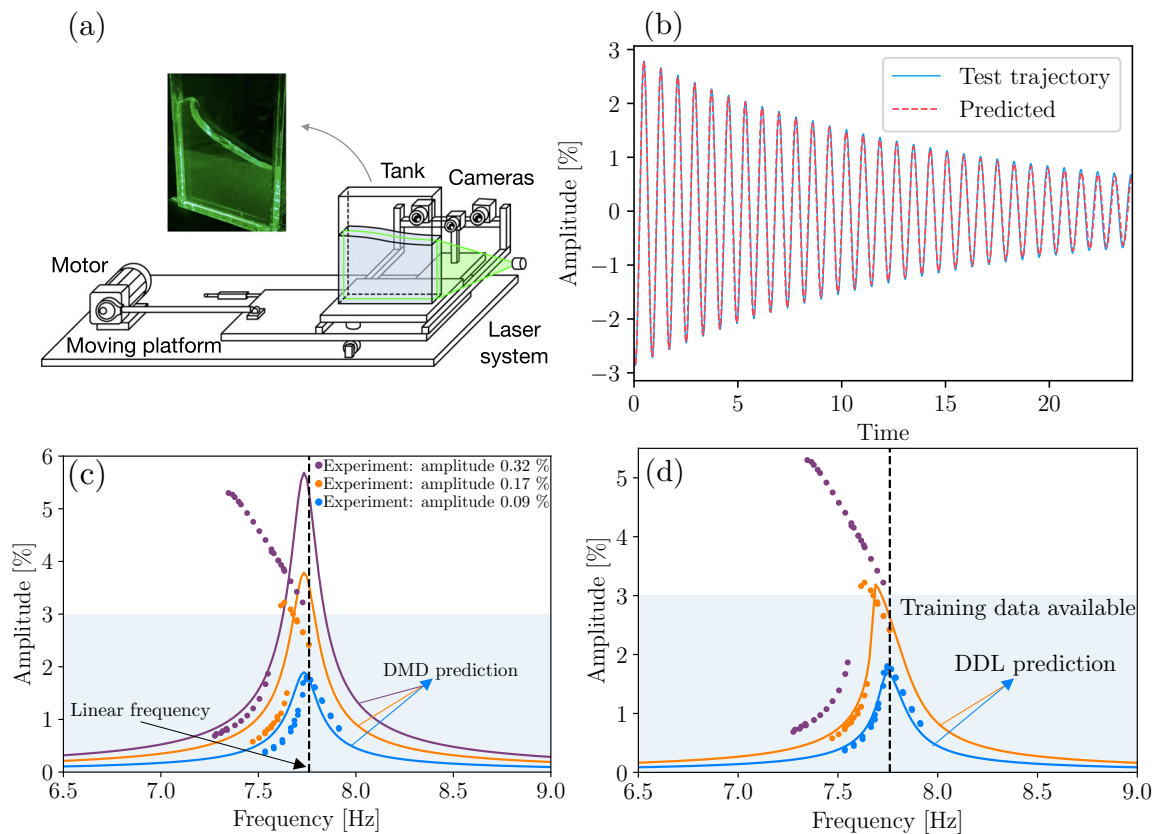


Figure 7: (a) Schematic representation of the experimental setup (adopted from Cenedese et al. [12]). (b) Prediction of the decay of a test trajectory with order- $k = 5$ DDL. (c) Prediction of the forced response from DMD. (d) Prediction of the forced response from DDL. Light shading indicates the domain, in which training data for DMD and DDL was available.

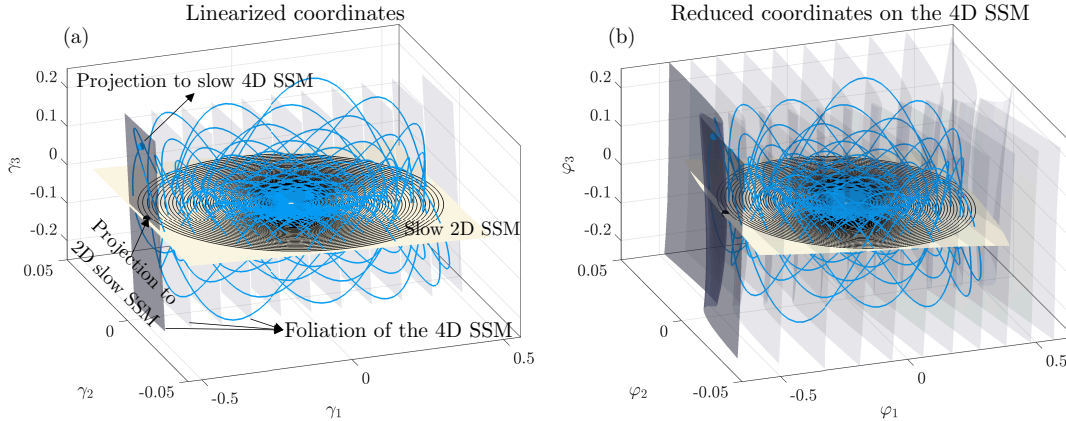


Figure 8: Reduced coordinates of the 4D SSM $\mathcal{W}(E)$ for the oscillator chain. The slow 2D SSM $\mathcal{W}(E_1)$, a typical trajectory and its projection to the slow SSM along the fibers $\mathcal{F}_{\mathbf{q}_0^{2D}}^0$ are also shown. Panel (a) shows the linearized coordinates computed from DDL, and (b) shows their image under the inverse of the linearizing transformation. The order of approximation used in DDL is 3.

a given trajectory close to $\mathcal{W}(E)$ ultimately synchronizes, we need to project along a point \mathbf{q}_0 of the full trajectory $\mathbf{q}(t)$ first onto $\mathcal{W}(E)$ orthogonally to obtain a point $\mathbf{q}_0^{4D} \in \mathcal{W}(E)$. We then need to identify the stable fiber $\mathcal{F}_{\mathbf{q}_0^{2D}}$ in $\mathcal{W}(E)$ for which $\mathbf{q}_0^{4D} \in \mathcal{F}_{\mathbf{q}_0^{2D}}$ holds. Finally, one has to project along $\mathcal{F}_{\mathbf{q}_0^{2D}}$ to locate its base point $\mathbf{q}_0^{2D} \in \mathcal{W}(E_1)$. The trajectory through \mathbf{q}_0^{2D} in $\mathcal{W}(E_1)$ will then be the one with which the full trajectory $\mathbf{q}(t)$ will synchronize faster than with any other trajectory. As noted in Section 4.3.3, computing the full nonlinear stable foliation

$$\mathcal{W}(E) = \bigcup_{\mathbf{q}_0^{2D} \in \mathcal{W}(E_1)} \mathcal{F}_{\mathbf{q}_0^{2D}}^0 \quad (67)$$

of $\mathcal{W}(E)$ is simple in the linearized coordinates, in which it can be achieved via a linear projection along the faster eigenspace E_2 .

We use a third-order polynomial approximation for $\mathcal{W}(E)$ based on the three training trajectories. The polynomials depend on the reduced coordinates we introduce along E using a singular value decomposition of the trajectory data. These reduced coordinates are shown in Fig. 8, where we show a representative training trajectory, the 2D slow SSM E_1 , as well as the foliation (67) computed from DDL for this specific problem.

We also evaluate the DDL-based predictions on $\mathcal{W}(E)$ and $\mathcal{W}(E_1)$ by comparing them to predictions from DMD and EDMD. Performing DMD and EDMD with the data first projected to E can be interpreted as finding the linear approximation to the dynamics in $\mathcal{W}(E)$. Similarly, performing DMD and EDMD with the data first projected to E_1 can be interpreted as finding the linear approximation to the dynamics in $\mathcal{W}(E_1)$. These are to be contrasted with performing DDL that finds the linearized reduced dynamics within $\mathcal{W}(E)$, which in turn contains the linearized reduced dynamics within $\mathcal{W}(E_1)$. Figure 9 shows that DMD and EDMD both perform similarly to DDL on $\mathcal{W}(E)$. However, the 2D DMD and EDMD results obtained for $\mathcal{W}(E_1)$ are noticeably less accurate than the DDL results.

6 Conclusions

We have given a new mathematical justification for the broadly used DMD procedure to eliminate the shortcomings of prior proposed justifications. Specifically, we have shown that under specific

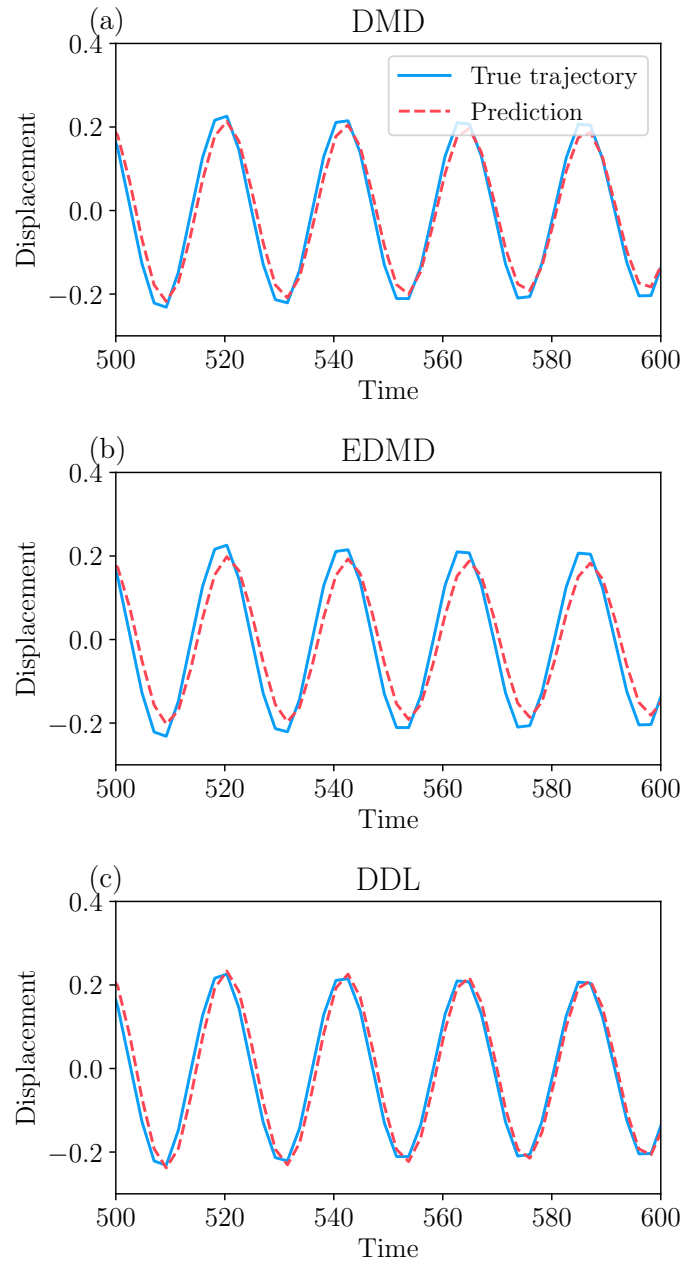


Figure 9: Predictions of (a) DMD (b) EDMD and (c) DDL models on a test trajectory of the oscillator chain. The order of approximation for DDL and EDMD is $k = 3$.

non-degeneracy conditions on the n -dimensional dynamical system, on $d \leq n$ observable functions defined for that system, and on the actual data from these observables, DMD gives a leading-order approximation to the observable dynamics on an attracting d -dimensional spectral submanifold (SSM) of the system.

This result covers both discrete and continuous dynamical systems even for $n = \infty$. Our Theorem 1 only makes explicit non-degeneracy assumptions on the observables which will hold with probability one in practical applications. This is to be contrasted with prior approaches to DMD and its variants based on the Koopman operator, whose assumptions on the observables fail with probability one on generic observables.

Our approach also yields a systematic procedure that gradually refines the leading-order DMD approximation of the reduced observable dynamics on SSMs to higher orders. This procedure, which we call data-driven linearization (DDL), builds a nonlinear coordinate transformation under which the observable becomes linear on the attracting SSM. We have shown on several examples how DDL indeed outperforms DMD and extended DMD (EDMD), as expected. In addition to this performance increase, DDL also enables a prediction of truly nonlinear forced response from unforced data within its training range. Although we have only illustrated this for periodically forced water sloshing experiments in a tank, recent results on aperiodically time-dependent SSMs by Haller and Kaundinya [20] allow us to predict more general forced response using DDL trained on unforced observable data.

Despite all these advantages, DDL (as any linearization method) remains applicable only in parts of the phase space where the dynamics are linearizable. Yet SSMs continue to exist across basin boundaries and hence are able to carry characteristically nonlinear dynamics with multiple coexisting attractors. For such nonlinearizable dynamics, data-driven nonlinear SSM-reduction algorithms, such as SSMLearn and fastSSM, are preferable and have been showing high accuracy and predictive ability in a growing number of physical settings (see, e.g., Cenedese et al. [12, 13], Axås et al. [3], Kaszás et al. [27], Alora et al. [1], Kaszás and Haller [26], Liu et al. [37]).

Acknowledgement We are grateful to Matthew Kvalheim and Shai Revzen for several helpful comments on an earlier version of this manuscript.

Funding This work was supported by the Swiss National Science Foundation.

Data Availability All data and codes used in this work are downloadable from the repository <https://github.com/haller-group/DataDrivenLinearization>.

Competing Interests The authors declare that they have no conflict of interest.

References

- [1] J.I. Alora, M. Cenedese, E. Schmerling, G. Haller, and M. Pavone. Practical deployment of spectral submanifold reduction for optimal control of high-dimensional systems. *IFAC PapersOnLine*, 56-2:4074–4081, 2023.
- [2] J. Axås and G. Haller. Model reduction for nonlinearizable dynamics via delay-embedded spectral submanifolds. *Nonlinear Dyn.*, 2023.

- [3] J. Axâs, M. Cenedese, and G. Haller. Fast data-driven model reduction for nonlinear dynamical systems. (<https://doi.org/10.1007/s11071-022-08014-0>), 2022.
- [4] D. M. Bates and D. G. Watts. *Nonlinear Regression Analysis and Its Applications*. Wiley, 1988.
- [5] B. Bäuerlein and K. Avila. Phase lag predicts nonlinear response maxima in liquid-sloshing experiments. *J. Fluid Mech.*, 925, 2021.
- [6] L. Bettini, B. Kaszâs, Bernhard Zybach, Jürg Dual, and George Haller. Model reduction to spectral submanifolds via oblique projection. *Preprint*, 2024.
- [7] E. M. Bollt, Q. Li, F. Dietrich, and I. Kevrekidis. On matching, and even rectifying, dynamical systems through Koopman operator eigenfunctions. *SIAM J. Appl. Dyn. Sys.*, 17(2):1925–1960, 2018.
- [8] M. Budišić, R. Mohr, and I. Mezić. Applied Koopmanism. *Chaos*, 22:047510, 2012.
- [9] G. Buza. Spectral submanifolds of the Navier–Stokes equations. *SIAM J. Appl. Dyn. Sys.*, 23(2):1052–1089, 2024.
- [10] X. Cabré, E. Fontich, and R. de la Llave. The parameterization method for invariant manifolds i: Manifolds associated to non-resonant subspaces. *Indiana Univ. Math. J.*, 52(2):283–328, 2003.
- [11] M. Cenedese, J. Axâs, and G. Haller. SSMLearn. <https://github.com/haller-group/SSMLearn>, 2021.
- [12] M. Cenedese, J. Axâs, B. Bäuerlein, K. Avila, and G. Haller. Data-driven modeling and prediction of non-linearizable dynamics via spectral submanifolds. *Nature Comm.*, 198, 2022.
- [13] M. Cenedese, J. Axâs, H. Yang, M. Eriten, and G. Haller. Data-driven nonlinear model reduction to spectral submanifolds in mechanical systems. *Phil. Trans. R. Soc. A*, 380:20210194, 2022.
- [14] H. Dankowicz and F. Schilder. *Recipes for Continuation*. SIAM, 2013.
- [15] C. Domb and M. F. Sykes. On the susceptibility of a ferromagnetic above the curie point. *Proceedings of the Royal Society of London. Series A, Mathematical and Physical Sciences*, 240(1221):214–228, 1957.
- [16] S.M. Elbially. Local contractions of Banach spaces and spectral gap conditions. *J. Func. Anal.*, 182:108–150, 2001.
- [17] J. Eldering, M Kvalheim, and S. Revzen. Global linearization and fiber bundle structure of invariant manifolds. *Nonlinearity*, 31:4202–4245, 2018.
- [18] N. Fenichel. Persistence and smoothness of invariant manifolds for flows. *Indiana Univ. Math. J.*, 21(3):193–226, 1971.
- [19] J. Guckenheimer and P. Holmes. *Nonlinear Oscillations, Dynamical Systems and Bifurcation of Vector Fields*. Springer, New York, 1983.
- [20] G. Haller and R. Kaundinya. Nonlinear model reduction to temporally aperiodic spectral submanifolds. *Chaos*, 34: 043152, 2024.
- [21] G. Haller and S. Ponsioen. Nonlinear normal modes and spectral submanifolds: existence, uniqueness and use in model reduction. *Nonlinear Dyn.*, 86(3):1493–1534, 2016.
- [22] G. Haller, B. Kaszâs, A. Liu, and J. Axâs. Nonlinear model reduction to fractional and mixed-mode spectral submanifolds. *Chaos*, 33(6):063138, 2023.

- [23] P. Hartman. On local homeomorphisms of Euclidean spaces. *Bol. Soc. Mat. Mexicana*, 5: 220–241, 1960.
- [24] S. Jain, T. Thurner, M. Li, and G. Haller. SSMTTool 2.3: Computation of invariant manifolds and their reduced dynamics in high-dimensional mechanics problems. <https://doi.org/10.5281/zenodo.4614201>, pages 1417–1450, 2023.
- [25] Robert Jentzsch. Untersuchungen zur theorie der folgen analytischer funktionen. *Acta Mathematica*, 41:219–251, 1916.
- [26] B. Kaszas and G. Haller. Capturing the edge of chaos as a spectral submanifold in pipe flows. *J. Fluid. Mech.*, 979:A48, 2024.
- [27] B. Kaszas, M. Cenedese, and G. Haller. Dynamics-based machine learning of transitions in couette flow. *Phys. Rev. Fluids.*, 7:L082402, 2022.
- [28] B. Kaszas, and G. Haller. Data-Driven Linearization: Numerical Implementation. <https://github.com/haller-group/DataDrivenLinearization>, 2024.
- [29] Diederik Kingma and Jimmy Ba. Adam: A method for stochastic optimization. In *International Conference on Learning Representations (ICLR)*, 2015.
- [30] F. Kogelbauer and G. Haller. Rigorous model reduction for a damped-forced nonlinear beam model: An infinite-dimensional analysis. *J. Nonlin. Sci.*, 28:1109–1150, 2018.
- [31] B.O. Koopman. Hamiltonian systems and transformation Hilbert space. *Proc.Natl. Acad. Sci. USA*, 7:315–318, 1931.
- [32] J.N. Kutz, S.L. Brunton, B.W. Brunton, and J.L. Proctor. *Dynamic Mode Decomposition*. SIAM, Philadelphia, PA, 2016.
- [33] M.D. Kvalheim and P. Arathoon. Linearizability of flows by embeddings. *arXiv:2305.18288*, 2023.
- [34] M.D. Kvalheim and S. Revzen. Existence and uniqueness of global koopman eigenfunctions for stable fixed points and periodic orbits. *Physica D*, 425:132959, 2021.
- [35] Y. Lan and I. Mezic. Linearization in the large of nonlinear systems and Koopman operator spectrum. *Physica D*, 242:42–53, 2013.
- [36] Q. Li, F. Dietrich, E. M. Bollt, and I. G. Kevrekidis. Extended dynamic mode decomposition with dictionary learning: A data-driven adaptive spectral decomposition of the Koopman operator. *Chaos*, 27(10):103111, 10 2017.
- [37] A. Liu, J. Axas, and G. Haller. Data-driven modeling and forecasting of chaotic dynamics on inertial manifolds constructed as spectral submanifolds. *Chaos*, 34:033140, 2022.
- [38] Z. Liu, N. Ozay, and E.D. Sontag. On the non-existence of immersions for systems with multiple omega-limit sets. *IFAC-PapersOnLine*, 56(2):60–64, 2023.
- [39] Z. Liu, N. Ozay, and E.D. Sontag. Properties of immersions for systems with multiple limit sets with implications to learning Koopman embeddings. *arXiv:2312.17045*, pages 1–14, 2024.
- [40] I. Mezic. Analysis of fluid flows via spectral properties of the Koopman operator. *Ann. Rev. Fluid Mech.*, 45(1):357–378, 2013.
- [41] S. E. Newhouse. On a differentiable linearization theorem of Philip Hartman. *Contemporary Math.*, 692:209–262, 2017.

- [42] S. E. Otto, A. Padovan, and C. W. Rowley. Optimizing oblique projections for nonlinear systems using trajectories. *SIAM J. Sci. Comput.*, 44(3):A1681–A1702, 2022.
- [43] S. E. Otto, A. Padovan, and C. W. Rowley. Model reduction for nonlinear systems by balanced truncation of state and gradient covariance. *SIAM J. Sci. Comput.*, 45(5):A2325–A2355, 2023.
- [44] J. Page and R.R. Kerswell. Koopman mode expansions between simple invariant solutions. *J. Fluid Mech.*, 879:1–27, 2019.
- [45] Adam Paszke, Sam Gross, Soumith Chintala, Gregory Chanan, Edward Yang, Zachary DeVito, Zeming Lin, Alban Desmaison, Luca Antiga, and Adam Lerer. Automatic differentiation in pytorch. In *NIPS-W*, 2017.
- [46] H. Poincaré. *Les Méthodes Nouvelles de la Mécanique Céleste*. Gauthier-Villars et Fils, Paris, 1892.
- [47] S. Ponsioen, T. Pedergnana, and G. Haller. Automated computation of autonomous spectral submanifolds for nonlinear modal analysis. *J. Sound Vibr.*, 420:269–295, 2018.
- [48] C. W. Rowley. Model reduction for fluids, using balanced proper orthogonal decomposition. *Int. J. Bifurcat. Chaos*, 15(03):997–1013, 2005.
- [49] C.W. Rowley, I. Mezić, S. Bagheri, P. Schlachter, and D.S. Henningson. Spectral analysis of nonlinear flows. *J. Fluid Mech.*, 641:115–127, 2009.
- [50] P.J. Schmid. Dynamic mode decomposition of numerical and experimental data. *J. Fluid Mech.*, 656:5–28, 2010.
- [51] P.J. Schmid. Dynamic mode decomposition and its variants. *Ann. Rev. Fluid Mech.*, 54:225–254, 2022.
- [52] S. Sternberg. Local contractions and theorem of Poincaré. *Am. J. Math.*, 79(4):809–824, 1957.
- [53] S. Sternberg. On the structure of local homeomorphisms of Euclidean n-space, II. *Am. J. Math.*, 80(3):623–631, 1958.
- [54] B. Szaksz. *The Stabilizing and Destabilizing Effects of Time Delays in Nonlinear Dynamical Systems*. Ph.D. Thesis, Budapest University of Technology and Economics, 2024.
- [55] R. Szalai. Invariant spectral foliations with applications to model order reduction and synthesis. *Nonlin. Dyn.*, 101:2645–2669, 2020.
- [56] S. van Strien. Smooth linearization of hyperbolic fixed points without resonance conditions. *J. Diff. Eqs.*, 85(1):66–90, 1990.
- [57] Pauli Virtanen, Ralf Gommers, Travis E. Oliphant, Matt Haberland, Tyler Reddy, David Cournapeau, Evgeni Burovski, Pearu Peterson, Warren Weckesser, Jonathan Bright, Stéfan J. van der Walt, Matthew Brett, Joshua Wilson, K. Jarrod Millman, Nikolay Mayorov, Andrew R. J. Nelson, Eric Jones, Robert Kern, Eric Larson, C J Carey, İlhan Polat, Yu Feng, Eric W. Moore, Jake VanderPlas, Denis Laxalde, Josef Perktold, Robert Cimrman, Ian Henriksen, E. A. Quintero, Charles R. Harris, Anne M. Archibald, António H. Ribeiro, Fabian Pedregosa, Paul van Mulbregt, and SciPy 1.0 Contributors. SciPy 1.0: Fundamental Algorithms for Scientific Computing in Python. *Nature Methods*, 17:261–272, 2020.
- [58] M.O. Williams, I.G. Kevrekidis, and C.W. Rowley. A data-driven approximation of the Koopman operator: Extending dynamic mode decomposition. *J. Nonlin. Sci.*, 9:1307–1346, 2015.
- [59] M.O. Williams, C.W. Rowley, and I.G. Kevrekidis. A kernel-based method for data-driven Koopman spectral analysis. *J. Comp. Dyn.*, 2:247–265, 2015.

- [60] Z. Wu, S. L. Brunton, and S. Revzen. Challenges in dynamic mode decomposition. *J. Royal Soc. Interface*, 18(185):20210686, 2021.

Supplementary Information for

Data-Driven Linearization of Dynamical Systems

George Haller³ and Bálint Kaszás
 Institute for Mechanical Systems
 ETH Zürich
 Leonhardstrasse 76, 8092 Zürich, Switzerland

A DMD and the Koopman operator

A.1 Observable dynamics and the Koopman operator

A classic approach, introduced first by Koopman [31] and revived recently by multiple authors (see, e.g., by Budišić et al. [8], Mezić [40], Kutz et al. [32] and the references cited therein), describes observable evolution via the Koopman operator $\mathcal{K}^t: \mathcal{G}^d \rightarrow \mathcal{G}^d$, defined on a Banach space \mathcal{G}^d of d -dimensional observable functions as the pull-back operation on observables under the flow map \mathbf{F}^t of system (1). Specifically,

$$\mathcal{K}^t[\phi](\mathbf{x}_0) := \phi(\mathbf{F}^t(\mathbf{x}_0)), \quad (68)$$

or, in more compact notation,

$$\mathcal{K}^t[\phi] = \phi \circ \mathbf{F}^t, \quad \phi \in \mathcal{G}^d. \quad (69)$$

As \mathcal{G}^d is a complete vector space, linear combinations of ℓ observables $\phi_1, \dots, \phi_\ell \in \mathcal{G}^d$ are also observables in \mathcal{G}^d and hence \mathcal{K}^t can be evaluated on them. Such an evaluation gives

$$\mathcal{K}^t(c_1\phi_1 + \dots + c_\ell\phi_\ell)(\mathbf{x}_0) = c_1\mathcal{K}^t[\phi_1](\mathbf{x}_0) + \dots + c_\ell\mathcal{K}^t[\phi_\ell](\mathbf{x}_0) \quad (70)$$

This last equation shows that the mapping \mathcal{K}^t is linear with respect to the choice of observables while the system's initial condition \mathbf{x}_0 is kept fixed. In contrast, DMD seeks to find an approximate mapping that is linear with respect to the choice of the system's initial conditions while the observable is kept fixed. Indeed, in applications of DMD, eq. (6) is posed for a fixed observable vector evaluated on various initial conditions. EDMD is also trained on system trajectories launched from different initial conditions, observed under the same general function of an initially fixed set of observables.

On a broader note, the linearity of the Koopman operator with respect to changes in the choice of an observable, as seen in eq. (70), does not imply linear dynamics for observations of the system under a fixed observable. For instance, let $\phi_1(\mathbf{x})$ denote the observation of the displacement, measured in meters, of the end point of a nonlinear beam whose current state in its phase space is denoted by \mathbf{x} . If, instead, we want to observe the position of the endpoint in millimeters, then we switch the observable $\phi_2(\mathbf{x}) = 10^3\phi_1(\mathbf{x})$, and hence for the observed initial state \mathbf{x}_0 of the beam, we have the change

$$\phi_2(\mathbf{x}_0) = c\phi_1(\mathbf{x}_0), \quad c = 10^3,$$

in the initial observation. It is then no surprise that this change in the initial observable will transform to the same change in the current observations of the endpoint at time t , i.e.,

$$\mathcal{K}^t[\phi_2](\mathbf{x}_0) = c\mathcal{K}^t[\phi_1](\mathbf{x}_0).$$

This simple fact, however, just reflects that the final results at time t change by the same multiple as their initial conditions if we decide to change the physical units in our measurements. Clearly, this fact does not imply any linear dynamics for the displacement of the endpoint of the beam. Indeed, $\mathcal{K}^t[\phi_2](\mathbf{x}_0)$ may well be a chaotic signal.

³Corresponding author. Email: georgehaller@ethz.ch

Another example would be tracking the total population of a continent and denoting the current state of the population by \mathbf{x} . Let $\phi_1(\mathbf{x})$ denote specifically the observable returning the population of country A and $\phi_2(\mathbf{x})$ denote the observable returning the population of country B within the same continent. If we decide now to jointly observe the population of these two countries, then we are in effect passing to a third observable at initial state \mathbf{x}_0 to obtain

$$\phi_3(\mathbf{x}_0) = \phi_2(b_0) + \phi_1(\mathbf{x}_0),$$

for the initial observations. To obtain the total population of countries A and B at the current state \mathbf{x} of the total population, we can simply write

$$\mathcal{K}^t[\phi_3](\mathbf{x}_0) = \mathcal{K}^t[\phi_1](\mathbf{x}_0) + \mathcal{K}^t[\phi_2](\mathbf{x}_0).$$

Again, this fact by itself does not say anything about the linearity or nonlinearity of the population growth in either country A or country B .

Finally, *the Koopman operator is as much nonlinear as it is linear with respect to the changes in the observables* as it commutes with any nonlinear single or multi-variable function of observables, as long as that function is also an observable. Indeed, for any function

$$\mathbf{g}: (\mathcal{G}^d)^\ell \rightarrow \mathcal{G}^d,$$

the observable $\psi(\mathbf{x}_0) = \mathbf{g}(\phi_1(\mathbf{x}_0), \dots, \phi_\ell(\mathbf{x}_0))$ satisfies

$$\mathcal{K}^t[\mathbf{g}(\phi_1, \dots, \phi_\ell)] = \mathbf{g}(\mathcal{K}^t[\phi_1], \dots, \mathcal{K}^t[\phi_\ell]).$$

To illustrate this general property of the Koopman operator, let \mathbf{x} denote the instantaneous velocity field of a 2D Navier-Stokes flow with density ρ and let $\phi_{ij}(\mathbf{x}) = |v_{ij}|$ be the specific velocity magnitude along the (i, j) location of a fixed spatial grid. If we now want to track the local kinetic energy of the flow at (i, j) , we do not have to reformulate and re-solve the Navier-Stokes equation for $\phi_{\text{kin}}(\mathbf{x}) = \frac{1}{2}\rho\phi_{ij}^2(\mathbf{x}) = |x_{ij}|^2$. Rather, we can use our already available observations of $\phi_{ij}(\mathbf{x})$ of the velocity field starting from an initial velocity field \mathbf{x}_0 to obtain $\mathcal{K}^t[\phi_{\text{kin}}](\mathbf{x}_0) = \frac{1}{2}\rho[\mathcal{K}^t[\phi_{ij}](\mathbf{x}_0)]^2$. This, however, does not imply a statement that “the dynamics of the 2D Navier-Stokes equation are quadratic in the space of observables”.

A.2 Differential equation for the dynamics of observables under the Koopman operator

We can directly verify that

$$\mathcal{K}^{t_1+t_2}\phi = \mathcal{K}^{t_2}\mathcal{K}^{t_1}\phi = \mathcal{K}^{t_1}\mathcal{K}^{t_2}\phi, \quad (\mathcal{K}^t)^{-1}\phi = \mathcal{K}^{-t}\phi,$$

i.e., \mathcal{K}^t defines a flow map on the observable space \mathcal{G}^d , as long as system (1) generates a flow \mathbf{F}^t on the phase space \mathcal{P} . To describe the dynamics generated by this flow map, let us select an arbitrary scalar observable $\phi \in \mathcal{G}^d$ and differentiate the defining relation (68) with respect to t to obtain

$$\frac{d}{dt}\{\mathcal{K}^t[\phi](\mathbf{x}_0)\} = D\phi(\mathbf{F}^t(\mathbf{x}_0))\mathbf{f}(\mathbf{F}^t(\mathbf{x}_0)). \quad (71)$$

Since we have

$$D_{\mathbf{x}_0}\phi(\mathbf{F}^t(\mathbf{x}_0)) = D\phi(\mathbf{F}^t(\mathbf{x}_0))D\mathbf{F}^t(\mathbf{x}_0),$$

and \mathbf{F}^t is a diffeomorphism, we can rewrite (71) as

$$\frac{d}{dt}\{\mathcal{K}^t[\phi](\mathbf{x}_0)\} = D_{\mathbf{x}_0}\phi(\mathbf{F}^t(\mathbf{x}_0))[D\mathbf{F}^t(\mathbf{x}_0)]^{-1}\mathbf{f}(\mathbf{F}^t(\mathbf{x}_0)) = D_{\mathbf{x}_0}\{\mathcal{K}^t[\phi](\mathbf{x}_0)\}[D\mathbf{F}^t(\mathbf{x}_0)]^{-1}\mathbf{f}(\mathbf{F}^t(\mathbf{x}_0)). \quad (72)$$

Note, however, that

$$[D\mathbf{F}^t(\mathbf{x}_0)]^{-1} \mathbf{f}(\mathbf{F}^t(\mathbf{x}_0)) = \mathbf{f}(\mathbf{x}_0), \quad (73)$$

where we used the fact that $\mathbf{f}(\mathbf{F}^t(\mathbf{x}_0))$ is a solution of the equation of variations $\dot{\boldsymbol{\xi}} = D\mathbf{F}^t(\mathbf{x}_0)\boldsymbol{\xi}$ and hence we have $\mathbf{f}(\mathbf{F}^t(\mathbf{x}_0)) = D\mathbf{F}^t(\mathbf{x}_0)\mathbf{f}(\mathbf{x}_0)$. Therefore, we obtain from eqs. (72) and (73) that

$$\frac{d}{dt}(\mathcal{K}^t \phi) = \mathcal{L}\mathcal{K}^t \phi \quad (74)$$

with the Liouville operator $\mathcal{L} : \mathcal{G}^d \mapsto \mathcal{G}^d$ defined as

$$\mathcal{L} : \phi \mapsto \mathcal{L}\phi := D\phi \mathbf{f}.$$

A.3 An example: The phase space variable as observable

As an illustration of the solution structure of the functional differential equation (74), consider the simplest nontrivial case wherein the observable function ϕ is just the identity map on $\mathcal{P} = \mathbb{R}^d$, i.e., $\hat{\phi} = \mathbf{I} : \mathbb{R}^d \rightarrow \mathbb{R}^d$. In that case, we specifically have the expressions

$$\hat{\phi}(\mathbf{x}_0) = \mathbf{x}_0, \quad \mathcal{K}^t \hat{\phi}(\mathbf{x}_0) = \mathbf{F}^t(\mathbf{x}_0), \quad \frac{d}{dt} \left\{ \mathcal{K}^t \hat{\phi} \right\} = \dot{\mathbf{F}}^t(\mathbf{x}_0) = \dot{\mathbf{x}}, \quad D_{\mathbf{x}_0} \left\{ \mathcal{K}^t \hat{\phi}(\mathbf{x}_0) \right\} = D\mathbf{F}^t(\mathbf{x}_0).$$

Substituting these formulas into the functional differential equation (74), we obtain

$$\dot{\mathbf{x}} = D\mathbf{F}^t(\mathbf{x}_0)\mathbf{f}(\mathbf{x}_0) = \mathbf{f}(\mathbf{x}). \quad (75)$$

Therefore, for the most commonly used observable in classic dynamical systems, the phase space variable \mathbf{x} , the linear functional differential equation (74) simplifies to the original nonlinear ODE ((1)).

This again underscores that the linearity of the Koopman operator does not imply linear dynamics for individual observations $\mathbf{x}(t; \mathbf{x}_0)$ of the evolution of the initial condition \mathbf{x}_0 . Rather, it implies that for any real constant c , the scaled initial observation $\tilde{\phi}(\mathbf{x}_0) = c\hat{\phi}(\mathbf{x}_0)$ of \mathbf{x}_0 will evolve into the identically scaled current observation $\mathcal{K}^t \tilde{\phi}(\mathbf{x}_0) = c\mathcal{K}^t \hat{\phi}(\mathbf{x}_0) = c\mathbf{x}(t; \mathbf{x}_0)$ of the trajectory at time t , i.e., \mathcal{K}^t will return $\mathbf{x}(t; \mathbf{x}_0)$ scaled by the same constant c . Most importantly, we will still generally have

$$\mathbf{x}(t; c\mathbf{x}_0) \neq c\mathbf{x}(t; \mathbf{x}_0),$$

unless the dynamical system (75) is linear. Therefore, the dynamics of the fixed observable $\mathbf{x}(t; \mathbf{x}_0)$ is not linear in the usual sense, i.e., with respect to changes in initial conditions. Rather, it is linear with respect to changes in the observable in which the evolution of the same trajectory is observed.

Equation (75) also illustrates that passing from the autonomous nonlinear ODE (1) to the functional differential equation (74) gives as infinite-dimensional linear formulation that is at least as complicated to solve as the original finite-dimensional nonlinear ODE formulation.

A.4 Koopman eigenfunctions

There are, nevertheless, non-generic sets of observables restricted to which e.q. (74) becomes a constant-coefficient linear system of ODEs. Examples are observables falling in the span of eigenfunctions of the Koopman operator \mathcal{K}^t , if and where such eigenfunctions exist.

Indeed, if for some constant $\lambda \in \mathbb{C}$, the eigenvalue problem

$$\mathcal{K}^t [\phi](\mathbf{x}_0) = e^{\lambda t} \phi(\mathbf{x}_0), \quad \mathbf{x}_0 \in \mathcal{D}, \quad (76)$$

has a solution $\phi : \mathcal{D} \rightarrow \mathbb{C}^d$ over some domain $\mathcal{D} \subset \mathcal{P}$ of the phase space, then we obtain

$$\frac{d}{dt} \mathcal{K}^t [\phi] = \lambda \mathcal{K}^t [\phi].$$

Consequently, if $\phi_1(\mathbf{x}_0), \dots, \phi_k(\mathbf{x}_0) \in \mathbb{C}^d$ are Koopman eigenfunctions with corresponding Koopman eigenvalues $\lambda_1, \dots, \lambda_k \in \mathbb{C}$ and domains of definition $\mathcal{D}_1, \dots, \mathcal{D}_k \subset \mathcal{P}$, then any observable $\mathbf{w} \in \oplus^d (\cap_{j=1}^k \mathcal{D}_j)$ of the form

$$\mathbf{w}(\mathbf{x}_0) = c_1 \phi_1(\mathbf{x}_0) + \dots + c_k \phi_k(\mathbf{x}_0) \quad (77)$$

satisfies

$$\mathcal{K}^t[\mathbf{w}] = \sum_{j=1}^k c_j \mathcal{K}^t[\phi_j] = \sum_{j=1}^k c_j e^{\lambda_j t} \phi_j.$$

Therefore, the coordinate representation $\mathbf{W}(t)$ of $\mathcal{K}^t[\mathbf{w}]$ in the basis ϕ_1, \dots, ϕ_j , given by

$$\mathbf{W}(t) = \begin{pmatrix} c_1 e^{\lambda_1 t} \\ \vdots \\ c_k e^{\lambda_k t} \end{pmatrix},$$

satisfies the k -dimensional autonomous linear ODE

$$\frac{d}{dt} \mathbf{W} = \mathbf{\Lambda} \mathbf{W}, \quad \mathbf{\Lambda} = \begin{pmatrix} \lambda_1 & 0 & 0 \\ 0 & \ddots & 0 \\ 0 & 0 & \lambda_k \end{pmatrix}.$$

More generally, if ϕ_1, \dots, ϕ_k are just linearly independent observables in the spectral subspace $\text{span}\{\phi_1, \dots, \phi_k\}$, then a similar ODE holds for W in the basis ϕ_1, \dots, ϕ_k . In that case, $\mathbf{\Lambda}$ is not a diagonal matrix but its eigenvalues are still $\lambda_1, \dots, \lambda_k$.

It is often forgotten, however, that Koopman eigenfunctions satisfying the eigenvalue problem (76) generally only exist on a subset \mathcal{D} of the phase space. This is made precise by the following simple observation:

Proposition 1. *At least one principal Koopman eigenfunction blows up (i.e., becomes unbounded) at the boundary of a domain of attraction or repulsion of a fixed point around which the underlying dynamical system admits a local C^1 linearization.*

Proof. We only prove the statement for domains of attraction of fixed points of continuous dynamical systems. Domains of repulsion can be handled in the same fashion in backward time and the proof for discrete dynamical systems is similar. Let \mathbf{x}_0 be a point on the boundary $\partial\mathcal{B}$ of a domain of attraction \mathcal{B} of a fixed point p of a continuous dynamical system. Then, arbitrarily close to \mathbf{x}_0 , there are initial conditions $\hat{\mathbf{x}}_0$ in the domain of attraction with arbitrarily long times of flight to the ball $B_\rho(p)$ around p in which the dynamical system can be C^1 linearized.

Lan and Mezic [35] extended local C^1 linearization near an attracting fixed point via the backward-time flow map to a global C^1 linearizing transformation $\mathbf{x} = \mathbf{h}(\mathbf{y})$ within \mathcal{B} that maps the original ODE within \mathcal{B} to $\dot{\mathbf{y}} = \mathbf{A}\mathbf{y}$ defined on \mathbb{R}^n . By the construction of this linearizing transformation, initial conditions $\hat{\mathbf{x}}_0$ whose times of flight to $B_\rho(p)$ is large will be mapped into initial conditions $\hat{\mathbf{y}}_0$ of the linearized system that are far from the origin $\mathbf{y} = \mathbf{0}$.

The unique principal Koopman eigenfunctions of the nonlinear system are known to be

$$\phi_j(\mathbf{x}) = \langle \mathbf{h}^{-1}(\mathbf{x}), \mathbf{v}_j \rangle, \quad j = 1, \dots, n, \quad (78)$$

with \mathbf{v}_j denoting the left eigenvectors of \mathbf{A} . As we have just concluded that $\mathbf{y} = \mathbf{h}^{-1}(\mathbf{x})$ will admit arbitrarily large values arbitrarily close to any point $\mathbf{x}_0 \in \partial\mathcal{B}$, it follows that there will be at least one j for which the principal Koopman eigenfunction $\phi_j(\mathbf{x})$ blows up at $\mathbf{x}_0 \in \partial\mathcal{B}$. \square

We note that the statement of Proposition 1 can also be deduced from the more general results in Theorem 3 of Kvalheim and Arathoon [33].

As a consequence of Proposition 1, one cannot simply patch together Koopman eigenfunctions outside boundaries of domains of attraction and thereby provide a viable Koopman-linearization for the whole phase space, as is often suggested. Indeed, even if found somehow, Koopman eigenfunctions would become unmanageable for the purposes of observer expansions even before reaching basin boundaries, as shown explicitly by the examples of Page and Kerswell [44].

B Proof of Theorem 1 and technical remarks

Under assumption (A1) of hyperbolicity of the theorem and under assumption (A2) on the smoothness class C^2 of the dynamical system, a refinement of the Hartman–Grobman theorem (see Guckenheimer and Holmes [19]) by Hartman [23] guarantees the local existence of a near-identity, linearizing change of coordinates of the form⁴

$$\mathbf{x} = \mathbf{y} + \mathbf{h}(\mathbf{y}), \quad \mathbf{y} \in U \subset \mathbb{R}^n, \quad \mathbf{h}(\mathbf{y}), \mathbf{h}^{-1}(\mathbf{y}) = \mathcal{O}\left(|\mathbf{y}|^{1+\beta}\right), \quad (79)$$

for some $\beta \in (0, 1)$, under which system (11) takes the exact linear form

$$\dot{\mathbf{y}} = \mathbf{A}\mathbf{y}. \quad (80)$$

As pointed out by Haller et al. [22] in the context of the more restrictive, C^∞ linearization theorem of Sternberg [53], the inverse of the linearizing transformation (79) maps the d -dimensional spectral subspace E of the linearized system (80) into a d -dimensional, normally attracting spectral submanifold (SSM),

$$\mathcal{W}(E) = (\mathbf{I} + \mathbf{h})^{-1}(E), \quad (81)$$

for system (11). The internal dynamics of this SSM govern the longer-term behavior of all trajectories near the origin. Generally, there will be infinitely many such invariant manifolds, but they are all tangent to E at the origin. We note that, $\mathcal{W}(E)$, as defined in eq. (81), is only known to be C^1 under our current set of assumptions. Under further nonresonance assumption on the spectrum of \mathbf{A} , the SSM can be shown to be as smooth as the underlying dynamical system (see Cabré et al. [10], Haller and Ponsioen [21]).

Based on these results, we apply the linearizing transformation (79) followed by a linear change of coordinates to $(\boldsymbol{\xi}, \boldsymbol{\eta})$, where $\boldsymbol{\xi}$ are coordinates along the spectral subspace E and $\boldsymbol{\eta}$ are coordinates along the spectral subspace F . Specifically, let

$$\mathbf{x} = \mathbf{T}\mathbf{y} + \mathbf{h}(\mathbf{T}\mathbf{y}), \quad \mathbf{y} = (\boldsymbol{\xi}, \boldsymbol{\eta})^T \in \mathbb{R}^d \times \mathbb{R}^{n-d}, \quad (82)$$

with the matrix \mathbf{T} defined in formula (15).

Under the transformation (82), the nonlinear system (11) becomes

$$\begin{pmatrix} \dot{\boldsymbol{\xi}} \\ \dot{\boldsymbol{\eta}} \end{pmatrix} = \begin{pmatrix} \boldsymbol{\Lambda}_E & 0 \\ 0 & \boldsymbol{\Lambda}_F \end{pmatrix} \begin{pmatrix} \boldsymbol{\xi} \\ \boldsymbol{\eta} \end{pmatrix}, \quad \boldsymbol{\Lambda}_E = (\mathbf{T}^{-1}\mathbf{A}\mathbf{T})|_E, \quad \boldsymbol{\Lambda}_F = (\mathbf{T}^{-1}\mathbf{A}\mathbf{T})|_F. \quad (83)$$

In these coordinates, the smoothest invariant manifold tangent to E is

$$\mathcal{W}(E) = \{(\boldsymbol{\xi}, \boldsymbol{\eta}) : \boldsymbol{\eta} = 0\},$$

within which the dynamics restricted to $\mathcal{W}(E)$ are then given by

$$\dot{\boldsymbol{\xi}} = \boldsymbol{\Lambda}_E \boldsymbol{\xi}. \quad (84)$$

⁴Hartman [23] only states that $h \in C^1$ in his main theorem. He adds, however, that his proof of the theorem also shows that Dh is uniformly Hölder continuous in U with Hölder exponent $\beta \in (0, 1)$, which implies eq. (79).

From eq. (83), we obtain the estimates

$$\begin{aligned} |\boldsymbol{\xi}(t; \boldsymbol{\xi}_0)| &\leq |\boldsymbol{\xi}_0| e^{(\text{Re}\lambda_1 + \epsilon_1)t}, \\ |\boldsymbol{\eta}(t; \boldsymbol{\eta}_0)| &\leq |\boldsymbol{\eta}_0| e^{(\text{Re}\lambda_{d+1} + \epsilon_{d+1})t}, \end{aligned}$$

where $\epsilon_j \geq 0$ is an arbitrarily small constant that can be chosen zero if the algebraic multiplicity of λ_j is equal to its geometric multiplicity.

With the help of the $(\boldsymbol{\xi}, \boldsymbol{\eta})$ coordinates and eq. (79), the class C^2 observable ϕ be locally be written as

$$\begin{aligned} \phi(x) &= \phi(\mathbf{T}\mathbf{y} + \mathbf{h}(\mathbf{T}\mathbf{y})) = D\phi(\mathbf{0})[\mathbf{T}\mathbf{y} + \mathbf{h}(\mathbf{T}\mathbf{y})] + \mathcal{O}(|\mathbf{y} + \mathbf{h}(\mathbf{y})|^2) \\ &= D\phi(\mathbf{0})\mathbf{T} \begin{pmatrix} \boldsymbol{\xi} \\ \boldsymbol{\eta} \end{pmatrix} + D\phi(\mathbf{0})\mathbf{h}(\mathbf{T}\mathbf{y}) + \mathcal{O}(|\boldsymbol{\xi}|^2, |\boldsymbol{\xi}||\boldsymbol{\eta}|, |\boldsymbol{\eta}|^2) \\ &= D\phi(\mathbf{0})\mathbf{T}_E\boldsymbol{\xi} + \mathcal{O}(|\boldsymbol{\eta}|) + \mathcal{O}(|(\boldsymbol{\xi}, \boldsymbol{\eta})|^{1+\beta}) + \mathcal{O}(|\boldsymbol{\xi}|^2, |\boldsymbol{\xi}||\boldsymbol{\eta}|, |\boldsymbol{\eta}|^2) \\ &= D\phi(\mathbf{0})\mathbf{T}_E\boldsymbol{\xi} + \mathcal{O}(|\boldsymbol{\eta}|) + \mathcal{O}(|(\boldsymbol{\xi}, \boldsymbol{\eta})|^{1+\beta}) \end{aligned} \quad (85)$$

for some $\beta \in (0, 1)$.

We also express the data matrix Φ defined in eq. (5) in terms of data matrices with respect to the coordinates $\mathbf{y} = (\boldsymbol{\xi}, \boldsymbol{\eta})$ by letting

$$\Phi = \phi(\mathbf{T}\mathbf{Y} - \mathbf{h}(\mathbf{T}\mathbf{Y})), \quad \mathbf{Y} = \begin{pmatrix} \Xi \\ \mathbf{H} \end{pmatrix}, \quad (86)$$

where the functions ϕ and \mathbf{h} are applied to the matrices involved column by column. From eqs. (85) and (86), we obtain that

$$\begin{aligned} \Phi &= D\phi(\mathbf{0})\mathbf{T}_E\Xi + \mathcal{O}(|\mathbf{H}|) + \mathcal{O}(|(\Xi, \mathbf{H})|^{1+\beta}), \\ \hat{\Phi} &= D\phi(\mathbf{0})\mathbf{T}_E e^{\Lambda_E \Delta t} \Xi + \mathcal{O}(|\mathbf{H}|) + \mathcal{O}(|(\Xi, \mathbf{H})|^{1+\beta}), \end{aligned} \quad (87)$$

where we have used the boundedness of the sampling time Δt and the near-identity nature of the linearizing mapping (82), which implies

$$\mathcal{O}(|\Xi|^\beta) = \mathcal{O}(|\mathbf{P}_E \mathbf{X}|^\beta), \quad \mathcal{O}(|\mathbf{H}|^\beta) = \mathcal{O}(|\mathbf{P}_F \mathbf{X}|^\beta). \quad (88)$$

From the equations (87), we obtain

$$\begin{aligned} \hat{\Phi}\Phi^T &= \left[D\phi(\mathbf{0})\mathbf{T}_E e^{\Lambda_E \Delta t} \Xi + \mathcal{O}(|\mathbf{H}|) + \mathcal{O}(|(\Xi, \mathbf{H})|^{1+\beta}) \right] \left[D\phi(\mathbf{0})\mathbf{T}_E \Xi + \mathcal{O}(|\mathbf{H}|) + \mathcal{O}(|(\Xi, \mathbf{H})|^{1+\beta}) \right]^T \\ &= D\phi(\mathbf{0})\mathbf{T}_E e^{\Lambda_E \Delta t} \Xi \Xi^T \mathbf{T}_E^T [D\phi(\mathbf{0})]^T + \mathcal{O}(|\mathbf{H}|^2, |\mathbf{H}||(\Xi, \mathbf{H})|^{1+\beta}, |(\Xi, \mathbf{H})|^{2+2\beta}), \\ (\Phi\Phi^T)^\dagger &= \left\{ \left[D\phi(\mathbf{0})\mathbf{T}_E \Xi + \mathcal{O}(|\mathbf{H}|) + \mathcal{O}(|(\Xi, \mathbf{H})|^{1+\beta}) \right] \left[D\phi(\mathbf{0})\mathbf{T}_E \Xi + \mathcal{O}(|\mathbf{H}|) + \mathcal{O}(|(\Xi, \mathbf{H})|^{1+\beta}) \right]^T \right\}^\dagger \\ &= \left[D\phi(\mathbf{0})\mathbf{T}_E \Xi \Xi^T \mathbf{T}_E^T [D\phi(\mathbf{0})]^T + \mathcal{O}(|\mathbf{H}|^2, |\mathbf{H}||(\Xi, \mathbf{H})|^{1+\beta}, |(\Xi, \mathbf{H})|^{2+2\beta}) \right]^\dagger. \end{aligned} \quad (89)$$

By the first assumption in (A4) of the theorem, $\Phi\Phi^T$ is invertible, and hence $(\Phi\Phi^T)^\dagger = (\Phi\Phi^T)^{-1}$. Therefore, by the second equation in (89), for small enough $|\Xi|$ and $|\mathbf{H}|$, the matrix $D\phi(\mathbf{0})\mathbf{T}_E \Xi \Xi^T \mathbf{T}_E^T [D\phi(\mathbf{0})]^T$ is also invertible and

$$(\Phi\Phi^T)^\dagger = \left[D\phi(\mathbf{0})\mathbf{T}_E \Xi \Xi^T \mathbf{T}_E^T [D\phi(\mathbf{0})]^T \right]^{-1} + \mathcal{O}(|\mathbf{H}|^2, |\mathbf{H}||(\Xi, \mathbf{H})|^{1+\beta}, |(\Xi, \mathbf{H})|^{2+2\beta}). \quad (90)$$

Then, by assumption (A3) of the theorem, we can write

$$\left(\Phi\Phi^T\right)^\dagger = \left(\mathbf{T}_E^T [D\phi(\mathbf{0})]^T\right)^{-1} \left(\Xi\Xi^T\right)^{-1} (D\phi(\mathbf{0})\mathbf{T}_E)^{-1} + \mathcal{O}\left(|\mathbf{H}|^2, |\mathbf{H}| |(\Xi, \mathbf{H})|^{1+\beta}, |(\Xi, \mathbf{H})|^{2+2\beta}\right). \quad (91)$$

Substitution of formulas (90)-(91) into eq. (8) gives

$$\begin{aligned} \mathcal{D} &= \hat{\Phi}\Phi^T \left(\Phi\Phi^T\right)^\dagger = \hat{\Phi}\Phi^T \left(\Phi\Phi^T\right)^{-1} \\ &= \left[D\phi(\mathbf{0})\mathbf{T}_E e^{\Lambda_E \Delta t} \Xi\Xi^T \mathbf{T}_E^T [D\phi(\mathbf{0})]^T + \mathcal{O}\left(|\mathbf{H}|^2, |\mathbf{H}| |(\Xi, \mathbf{H})|^{1+\beta}, |(\Xi, \mathbf{H})|^{2+2\beta}\right) \right] \\ &\quad \times \left[\left(\mathbf{T}_E^T [D\phi(\mathbf{0})]^T\right)^{-1} \left(\Xi\Xi^T\right)^{-1} (D\phi(\mathbf{0})\mathbf{T}_E)^{-1} + \mathcal{O}\left(|\mathbf{H}|^2, |\mathbf{H}| |(\Xi, \mathbf{H})|^{1+\beta}, |(\Xi, \mathbf{H})|^{2+2\beta}\right) \right] \\ &= D\phi(\mathbf{0})\mathbf{T}_E e^{\Lambda_E \Delta t} (D\phi(\mathbf{0})\mathbf{T}_E)^{-1} + \mathcal{O}\left(|\Xi|^{-2} |\mathbf{H}|^2, |\Xi|^{-2} |\mathbf{H}| |(\Xi, \mathbf{H})|^{1+\beta}, |\Xi|^{-2} |(\Xi, \mathbf{H})|^{2+2\beta}\right) \\ &= D\phi(\mathbf{0})\mathbf{T}_E e^{\Lambda_E \Delta t} (D\phi(\mathbf{0})\mathbf{T}_E)^{-1} + \mathcal{O}\left(|\Xi|^\beta\right), \end{aligned}$$

where we have use the second assumption in (A4) of the Theorem. This completes the proof of Theorem 1, given the order-of-magnitude relations (88).

Remark 4. In systems where the slowest decaying modes are oscillatory, the slow spectral subspace E is always even dimensional, as it is spanned by the real and imaginary parts of the generalized eigenvectors of \mathbf{A} that correspond to complex conjugate pairs of eigenvalues. For such predominantly oscillatory systems, therefore, the number d of observables used in DMD has to be an even number for assumption (A3) to hold.

Remark 5. In most applications the dynamical system will have higher degree of smoothness, i.e., we will have $\mathbf{f} \in C^r$ for some $r \in \mathbb{N}^+ \cup \{\infty, a\}$, with C^a referring to the space of analytic functions. Then, under further nonresonance conditions of the spectrum of \mathbf{A} , the spectral submanifold $\mathcal{W}(E)$ will also be of class C^r , as we discuss in Section 4. In those cases, for the approximate topological equivalence holds in the statement of Theorem 1 hold on the full domain of attraction of the $\mathbf{x} = \mathbf{0}$ fixed point within $\mathcal{W}(E)$, as one deduces from the linearization-in-the-large results of Lan and Mezic [35] and Kvalheim and Revzen [34].⁵ In Theorem 1, our objective was to give a minimal set of conditions under which DMD can be justified as an approximate, leading-order, d -dimensional reduced model for the original nonlinear system. These minimal conditions only require hyperbolicity, i.e., robustness of the spectrum under perturbations, without insisting on the lack of resonances in the spectrum. This is advantageous in data-driven applications in which details of the spectrum are generally not known.

Remark 6. As in the case of finite-dimensional systems, linearization theorems guaranteeing higher-degree of smoothness for the linearizing transformations are also available in infinite dimensions, but these require various non-resonance conditions on the spectrum of \mathbf{A} (see, e.g., Elbially [16]). In Theorem 3, as in the finite-dimensional case, our objective was to present a minimal set of assumptions under which DMD can be justified without the detailed knowledge of the spectrum of \mathbf{A} .

Remark 7. We note that the more general Theorem 1.5 of Newhouse [41] also shows $C^{1,\alpha}$ linearizability for a class of systems that have so called α -hyperbolic (as opposed to stable hyperbolic) fixed points. This would enable us to waive the requirement in Theorem 3 that \mathbf{A} is a contraction and also allow for expanding directions within the spectral subspace E , as we did in our remarks after Theorems 1 and 2. The defining properties of these α -hyperbolic systems are, however, complicated to verify and do not hold for general hyperbolic fixed points even in finite-dimensional Banach spaces.

⁵Note that these global linearization results rely on the existence of a C^1 local linearization, which generally only exists for class C^2 dynamical systems. Consequently, one cannot use the available global linearization results within $\mathcal{W}(E)$ under the general assumptions of Theorem 1, which only guarantee C^1 differentiability for the reduced flow in $\mathcal{W}(E)$.

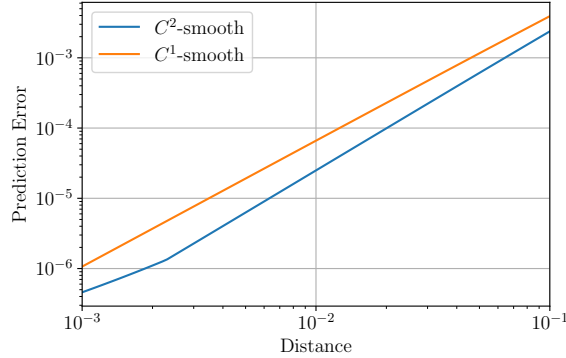


Figure 10: Prediction accuracy of DMD on C^1 - and C^2 -smooth systems (92). The orange curve shows the accuracy of DMD for $\alpha = 0.9$, while the blue curve corresponds to $\alpha = 1$.

For instance, the simple three-dimensional example of Hartman [23] (eq. (8) in that reference) of a non- C^1 linearizable system has a hyperbolic fixed point that is not α -hyperbolic in the sense of Newhouse [41].

C Necessity of assumptions (A2)-(A4) of Theorem 1

Assumption (A2) of Theorem 1 requires C^2 smoothness for the dynamical system (11). We now show on an example that if only C^1 smoothness holds for the dynamical system, then the DMD approximation can be less accurate. Consider the 1D system

$$\dot{x} = -x + x^{1+\alpha}. \quad (92)$$

The origin $x = 0$ is an asymptotically stable fixed point. For $\alpha > 0$, the system is C^1 at the origin, but the second derivative $\frac{\partial^2 \dot{x}}{\partial x^2} = \alpha^2 x^{\alpha-1}$ is singular at $x = 0$ for $\alpha < 1$. We compare the accuracy of a simple DMD prediction for $\alpha = 1$, which corresponds to C^2 smoothness and for $\alpha = 0.9$, which corresponds to only C^1 -smoothness at $x = 0$. The DMD prediction errors can be seen in Fig. 10 as a function of the initial distance of the trajectory from the origin. Although the C^1 -smooth system is close to the C^2 system, a large difference can be observed in the prediction accuracy of DMD asymptotically as $x \rightarrow 0$.

Assumption (A3) of Theorem 1 requires a specific nondegeneracy condition to hold for the observable in order for DMD to give a meaningful approximation. We now illustrate on an example what happens if this nondegeneracy condition is not satisfied. Consider the chain of nonlinear oscillators in Section 5.5. Let us denote the normal modes of the mechanical system (66) linearized around the stable fixed point $\mathbf{q} = \mathbf{0}$, as $\hat{\mathbf{q}}_j(t) = \hat{\mathbf{q}}_j(0)e^{\lambda_j t}$, where the mode shapes $\hat{\mathbf{q}}_j(0) \in \mathbb{R}^5$ satisfy

$$(\lambda_j^2 \mathbf{M} + \lambda_j \mathbf{C} + \mathbf{K}) \hat{\mathbf{q}}_j(0) = 0.$$

Therefore, in the phase space spanned by the variable

$$\mathbf{x} = (q_1, q_2, \dots, q_5, \dot{q}_1, \dots, \dot{q}_5) \in \mathbb{R}^{10},$$

the eigenvectors of the linear part of (66) are given as

$$\mathbf{e}_j = (\hat{\mathbf{q}}_j(0), \lambda_j \hat{\mathbf{q}}_j(0))^T.$$

With our choice of parameters, the slowest pair of eigenvalues are

$$\lambda_{1,2} = -0.0012 \pm i0.2825,$$

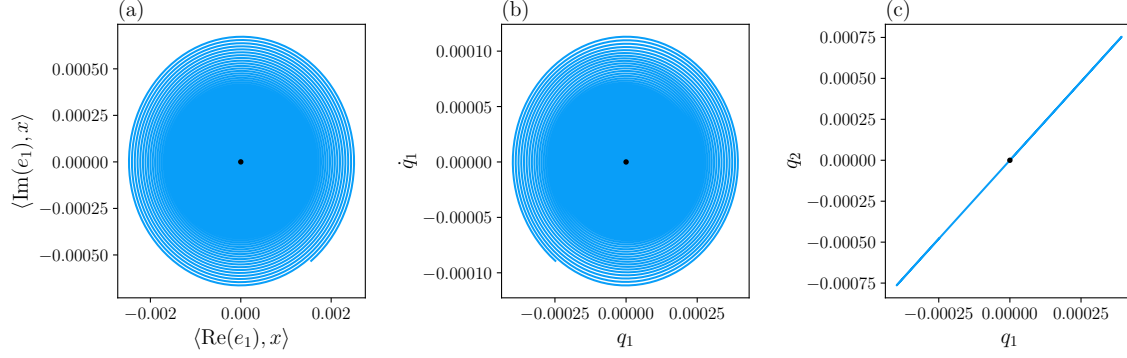


Figure 11: The dynamics near the $\mathbf{x} = \mathbf{0}$ point on the slow 2D SSM $\mathcal{W}(E)$ of system (66) represented via different observables (a) Observable $\phi_1(\mathbf{x})$ (b) Observable $\phi_2(\mathbf{x})$ (c) Observable $\phi_3(\mathbf{x})$.

and hence there exists a 2D slow SSM tangent to the slow spectral subspace

$$E = \text{span}([\text{Re}(\mathbf{e}_1), \text{Im}(\mathbf{e}_1)]) = \text{span}([\hat{\mathbf{q}}_1(0), \text{Re}(\lambda_1) \hat{\mathbf{q}}_1(0)], [0, \text{Im}(\lambda_1) \hat{\mathbf{q}}_1(0)]),$$

where \mathbf{e}_1 is the eigenvector corresponding to λ_1 .

As the dimension of $\mathcal{W}(E)$ is $d = 2$, we consider three possible 2D observables with respect to which Theorem 1 could potentially be applied:

$$\phi_1(\mathbf{x}) = \begin{pmatrix} \langle \text{Re}(\mathbf{e}_1), \mathbf{x} \rangle \\ \langle \text{Im}(\mathbf{e}_1), \mathbf{x} \rangle \end{pmatrix} \quad \phi_2(\mathbf{x}) = \begin{pmatrix} q_1 \\ \dot{q}_1 \end{pmatrix} \quad \phi_3(\mathbf{x}) = \begin{pmatrix} q_1 \\ q_2 \end{pmatrix}.$$

The Jacobians of these observables with respect to x can be computed as

$$\begin{aligned} D\phi_1(\mathbf{0}) &= (\text{Re}(\mathbf{e}_1) \text{Im}(\mathbf{e}_1))^T = \begin{pmatrix} * & * & * & \cdots & * \\ 0 & 0 & 0 & \cdots & * \end{pmatrix}, \\ D\phi_2(\mathbf{0}) &= \begin{pmatrix} 1 & 0 & 0 & \cdots & 0 \\ 0 & 1 & 0 & \cdots & 0 \end{pmatrix}, \\ D\phi_3(\mathbf{0}) &= \begin{pmatrix} 1 & 0 & 0 & \cdots & 0 \\ 0 & 0 & 1 & \cdots & 0 \end{pmatrix}, \end{aligned}$$

where $*$ denotes nonzero entries. Therefore, we require

$$\text{rank} [D\phi_{1,2,3}(\mathbf{0})|_E] = 2. \quad (93)$$

The restriction of the Jacobians of the observables to E is $D\phi_i(\mathbf{0})[\text{Re}(\mathbf{e}_1), \text{Im}(\mathbf{e}_1)]$. It can be seen from the structure of the matrices, that for ϕ_1 and ϕ_2 , the rank of the restricted Jacobian is 2, but for ϕ_3 , it is only of rank 1. Therefore, the observable vector ϕ_3 cannot be used to parametrize the SSM and to derive a reduced-order model.

Figures 11a-b show that observing the dynamics via $\phi_1(x)$ and $\phi_2(x)$ indeed results in a successful embedding of the dynamics on $\mathcal{W}(E)$ near the fixed point. At the same time, Fig. 11c shows that using the observable $\phi_3(x)$ does not correctly reproduce the dynamics near the origin.

Assumption (A4) of Theorem 1 states that the collected data has to be rich enough to a neighborhood of the SSM near the fixed point. To illustrate this, we modify the linear system in (59) to have three real eigenvalues by letting $\mathbf{\Lambda} = \text{diag}(a, b, c) \in \mathbb{R}^3$. We then collect the resulting trajectories in the phase space in the observable data matrix

$$\Phi = \begin{pmatrix} x_1(0) & ax_1(0) & \cdots & a^n x_1(0) \\ x_2(0) & bx_2(0) & \cdots & b^n x_2(0) \\ x_3(0) & cx_3(0) & \cdots & c^n x_3(0) \end{pmatrix}.$$

Assuming $c < b < a < 0$, we seek to identify from the data matrix Φ the 2D slow eigenspace $\mathcal{W}(E) = E$ corresponding to the eigenvalues a and b . Assume now that $x_2(0) = x_3(0) = 0$ holds. In this case, the second and third rows of Φ are identically zero and hence its rank is only 1, which violates assumption (A4) of Theorem 1. Indeed, the trajectory observed in Φ is restricted to the slowest 1D eigenspace $\mathcal{W}(E_1) = E_1$ corresponding to the eigenvalue a and hence cannot be used to approximate the shape and internal dynamics of $\mathcal{W}(E)$.

In practice, a generic trajectory of a nonlinear system would not be restricted to a lower-dimensional invariant subspace and hence the data matrix Φ would have full rank with probability one. However, if the available data is close to a lower-dimensional invariant subspace, the condition number of the data matrix may become prohibitively large. So a near-failure of assumption (A4) is already detrimental to the quality of the results obtained from DMD.

D Proof of Theorem 4

For $\mathbf{f}_2 \in C^r$ and under the nonresonance conditions

$$\lambda_k \neq \sum_{j=1}^n m_j \lambda_j, \quad j, k = 1, \dots, n, \quad \sum_{j=1}^n m_j \geq 2, \quad (94)$$

the C^∞ linearization theorems of Sternberg [52] and Poincaré [46] guarantee the local existence of a near-identity, linearizing change of coordinates of the form

$$\mathbf{x} = \mathbf{y} + \mathbf{h}(\mathbf{y}), \quad \mathbf{y} \in U \subset \mathbb{R}^n, \quad \mathbf{h}(\mathbf{y}), \mathbf{h}^{-1}(\mathbf{y}) = \mathcal{O}(|\mathbf{y}|^2), \quad (95)$$

with $\mathbf{h} \in C^r$. Additionally, a strengthening of Sternberg's linearization theorem by Kvalheim and Revzen [34]⁶ implies that the transformation in eq. (95) is unique and globally defined on the full domain of attraction of the fixed point at the origin. As pointed out by Haller et al. [22], this implies the existence of a unique d -dimensional, normally attracting spectral submanifold $\mathcal{W}(E) \in C^\infty$ for system (11) whose internal dynamics govern the longer-term behavior of all trajectories near the origin.⁷

By the main assumption of the theorem, we have $\operatorname{Re} \lambda_1 < 0$. Under this assumption, the infinitely many nonresonance conditions in (94) simplify to finitely many. Indeed, if we define the spectral quotient as the positive integer Q given by

$$Q = \left\lfloor \frac{\max_i |\operatorname{Re} \lambda_i|}{\min_i |\operatorname{Re} \lambda_i|} \right\rfloor + 1,$$

Then, for all $m_j \in \mathbb{N}$ with $\sum_{j=1}^n m_j > Q$, we have the estimate

$$\begin{aligned} \sum_{j=1}^n m_j \operatorname{Re} \lambda_j &\leq - \sum_{j=1}^n m_j \min_i |\operatorname{Re} \lambda_i| < - \sum_{j=1}^n m_j \frac{\max_i |\operatorname{Re} \lambda_i|}{Q} = - \max_i |\operatorname{Re} \lambda_i| \frac{\sum_{j=1}^n m_j}{Q} \\ &< - \max_i |\operatorname{Re} \lambda_i|, \end{aligned}$$

implying

$$\sum_{j=1}^n m_j \operatorname{Re} \lambda_j < \operatorname{Re} \lambda_k, \quad k = 1, \dots, n, \quad \sum_{j=1}^n m_j > Q. \quad (96)$$

⁶This generalizes the results of Lan and Mezic [35] in the setting of the C^1 linearization theorem by Hartman [23].

⁷Cabr e et al. [10] guarantees the existence and uniqueness of $\mathcal{W}(E) \in C^\infty$ under weaker nonresonance conditions that allow resonances inside E but no resonances of the form (94) with $\lambda_k \in \operatorname{Spect}(A|_F)$ and $\lambda_j \in \operatorname{Spect}(\mathbf{A}|_E)$. We do not rely on these results here, as the next step in our construction is local linearization within $\mathcal{W}(E)$, which cannot be carried out in the presence of resonances inside E .

Consequently, in this case, no integer resonance among the eigenvalues of \mathbf{A} can occur for $\sum_{j=1}^n m_j > Q$ and hence the nonresonance condition (94) can be relaxed to assumption (A1) of Theorem 4.

Based on these results, we apply the C^r linearizing transformation (95) followed by a linear change of coordinates to $(\boldsymbol{\xi}, \boldsymbol{\eta})$ uses in the proof of Theorem 1 (see eq. (82)). As we have seen there, this coordinate change maps the spectral submanifold $\mathcal{W}(E)$ into the $\boldsymbol{\eta} = \mathbf{0}$ plane. On $\mathcal{W}(E)$, the reduced dynamics obeys the linear ODE

$$\dot{\boldsymbol{\xi}} = \boldsymbol{\Lambda}_E \boldsymbol{\xi}, \quad \boldsymbol{\Lambda}_E = (\mathbf{T}^{-1} \mathbf{A} \mathbf{T})|_E, \quad (97)$$

where $\boldsymbol{\Lambda}_E$, the real Jordan canonical form of $\mathbf{A}|_E$, has eigenvalues $\lambda_1, \dots, \lambda_d$.

Restricted to $\mathcal{W}(E)$, we can express the d -dimensional observable vector $\boldsymbol{\phi}(\mathbf{x})$ as

$$\boldsymbol{\phi}(\boldsymbol{\xi}) = \boldsymbol{\phi} \left(\mathbf{T} \begin{pmatrix} \boldsymbol{\xi} \\ \mathbf{0} \end{pmatrix} + \mathbf{h} \begin{pmatrix} \boldsymbol{\xi} \\ \mathbf{0} \end{pmatrix} \right) \in \mathbb{R}^d. \quad (98)$$

On the manifold $\mathcal{W}(E)$, we can use $\boldsymbol{\varphi}$ locally near the origin as a new variable if the coordinate change from $\boldsymbol{\xi}$ to $\boldsymbol{\varphi}$ is a C^r diffeomorphism on $\mathcal{W}(E)$, i.e., $D_{\boldsymbol{\xi}} \boldsymbol{\varphi}$ is nonsingular at the origin. To see if this is the case, note that

$$D_{\boldsymbol{\xi}} \boldsymbol{\psi}(\boldsymbol{\xi}) = D\boldsymbol{\phi} \left(\mathbf{T} \begin{pmatrix} \boldsymbol{\xi} \\ \mathbf{0} \end{pmatrix} \right) \mathbf{T} \begin{pmatrix} \mathbf{I}_{d \times d} \\ \mathbf{0} \end{pmatrix},$$

which gives

$$D_{\boldsymbol{\xi}} \boldsymbol{\gamma}(\mathbf{0}) = D\boldsymbol{\phi}(\mathbf{0}) \mathbf{T} \begin{pmatrix} \mathbf{I}_{d \times d} \\ \mathbf{0} \end{pmatrix} = D\boldsymbol{\phi}(\mathbf{0}) \mathbf{T}_E,$$

with the operator \mathbf{T}_E defined in (15). By assumption (35) of the theorem, we have

$$\det [D\boldsymbol{\phi}(\mathbf{0}) \mathbf{T}_E] \neq 0, \quad (99)$$

and hence, by the inverse function theorem, $\boldsymbol{\xi}$ can be expressed from the relationship (98) near the origin as a smooth function of $\boldsymbol{\varphi}$. Specifically, there exists a C^r diffeomorphism $\boldsymbol{\psi}: \mathbb{R}^d \rightarrow \mathbb{R}^d$ such that

$$\boldsymbol{\xi} = \boldsymbol{\psi}(\boldsymbol{\varphi}), \quad \boldsymbol{\psi}(\mathbf{0}) = \mathbf{0}, \quad D_{\boldsymbol{\varphi}} \boldsymbol{\psi}(\boldsymbol{\varphi}) = [D_{\boldsymbol{\xi}} \boldsymbol{\varphi}(\boldsymbol{\xi})]^{-1}. \quad (100)$$

Differentiating the first equation in (100), substituting eq. (97), using the relations (100) and Taylor expanding the result around $\boldsymbol{\varphi} = \mathbf{0}$, we obtain the reduced dynamics on $\mathcal{W}(E)$ in the form

$$\begin{aligned} \dot{\boldsymbol{\varphi}} &= [D_{\boldsymbol{\varphi}} \boldsymbol{\psi}(\boldsymbol{\varphi})]^{-1} \boldsymbol{\Lambda}_E \boldsymbol{\psi}(\boldsymbol{\varphi}) \\ &= D_{\boldsymbol{\xi}} \boldsymbol{\varphi}(\mathbf{0}) \boldsymbol{\Lambda}_E [D_{\boldsymbol{\xi}} \boldsymbol{\varphi}(\mathbf{0})]^{-1} \boldsymbol{\varphi} + \mathbf{q}(\boldsymbol{\varphi}), \quad \mathbf{q}(\boldsymbol{\varphi}) = o(|\boldsymbol{\varphi}|) \end{aligned} \quad (101)$$

for some C^r function $\mathbf{q}: U \subset \mathbb{R}^d \rightarrow \mathbb{R}^d$ defined in a neighborhood of $\boldsymbol{\varphi} = \mathbf{0}$. This proves statement (i) of the theorem.

We have seen that $D_{\boldsymbol{\xi}} \boldsymbol{\varphi}(\mathbf{0})$ is nonsingular and hence the linear part of the nonlinear ODE in (101) has the same eigenvalues as $\boldsymbol{\Lambda}_E$ does. $(\mathbf{T}^{-1} \mathbf{A} \mathbf{T})|_E$. Consequently, the origin of system (102) is a hyperbolic fixed point. If the nonresonance conditions (34) hold for the full spectrum of \mathbf{A} , then they also hold for any subset of this spectrum, i.e., for the eigenvalues of $\boldsymbol{\Lambda}_E$ as well. Consequently, from the linearization theorems of Sternberg [52] and Kvalheim and Revzen [34], we can also deduce a similar near-identity, C^r linearizing diffeomorphism

$$\boldsymbol{\varphi} = \boldsymbol{\gamma} + \boldsymbol{\ell}(\boldsymbol{\gamma}), \quad \boldsymbol{\ell}(\boldsymbol{\gamma}) = o(|\boldsymbol{\gamma}|), \quad \boldsymbol{\ell} \in C^r,$$

for $r \in \mathbb{N}^+ \cup \{\infty, a\}$ under the nonresonance assumption (34). In the new $\boldsymbol{\gamma}$ coordinates, the dynamics on the SSM $\mathcal{W}(E)$ is governed by the linear ODE

$$\dot{\boldsymbol{\gamma}} = D_{\boldsymbol{\xi}} \boldsymbol{\gamma}(\mathbf{0}) \boldsymbol{\Lambda}_E [D_{\boldsymbol{\xi}} \boldsymbol{\gamma}(\mathbf{0})]^{-1} \boldsymbol{\gamma}, \quad (102)$$

which proves statement (ii) of the theorem.

The partial differential equation (39) can then be obtained by differentiating eq. (37) and substituting eqs. (36) and (38) into the resulting equation. The expansions (40) and (41) then follow from the guaranteed smoothness class of the linearizing transformation for general r and for $r = a$, respectively. This concludes the proof of statement (iii) of the theorem.

E Reduced dynamics on periodically forced SSMs

Let us denote the time- T map for the periodically forced system by \mathbf{P}_ε^T . Since \mathbf{P}_0^T represents the period- T sampling of the flow map of the unperturbed system, it has a fixed point at $\mathbf{x} = \mathbf{0}$. By the implicit function theorem, \mathbf{P}_ε^T also has a fixed point $O(\varepsilon)$ -close to $\mathbf{x} = \mathbf{0}$. This corresponds to a periodic orbit of (52) close to the origin. As explained by Haller et al. [22], the C^∞ linearization results of Sternberg [52] and Poincaré [46] also establish the smoothness of the linearizations in ε . Applied to the discrete dynamical system defined by the Poincaré-map, these results guarantee the existence of a linearizing transformation of the form

$$\mathbf{x} = \mathbf{y} + \mathbf{h}^\varepsilon(\mathbf{y}), \quad \mathbf{y} \in U \subset \mathbb{R}^n, \quad \mathbf{h}(\mathbf{y}), \mathbf{h}^{-1}(\mathbf{y}) = \mathcal{O}\left(|\mathbf{y}|^2, \varepsilon|\mathbf{y}|^2\right),$$

with $\mathbf{h} \in C^r$ in both \mathbf{y} and ε .

We now apply the ε -dependent linearizing transformation followed by the linear change of coordinates to the coordinates $(\boldsymbol{\xi}, \boldsymbol{\eta})$ introduced in the proof of Theorem 4. Specifically, let

$$\mathbf{x} = \mathbf{T}\mathbf{y} + \mathbf{h}^\varepsilon(\mathbf{T}\mathbf{y}), \quad \mathbf{y} = (\boldsymbol{\xi}, \boldsymbol{\eta})^T \in \mathbb{R}^d \times \mathbb{R}^{n-d}, \quad (103)$$

with the matrix \mathbf{T} defined in formula (15), i.e., containing eigenvalues of \mathbf{A} . As the change of coordinates (103) is smooth in ε , it can be written as $\mathbf{x} = \mathbf{T}\mathbf{y} + \mathbf{h}^0(\mathbf{T}\mathbf{y}) + O(|\mathbf{y}|^2\varepsilon)$. Differentiation of (103) with respect to time yields

$$\dot{\mathbf{x}} = (\mathbf{T} + D\mathbf{h}^\varepsilon(\mathbf{T}\mathbf{y})\mathbf{T})\dot{\mathbf{y}} = \mathbf{A}(\mathbf{T}\mathbf{y} + \mathbf{h}^\varepsilon(\mathbf{T}\mathbf{y})) + \tilde{\mathbf{f}}(\mathbf{T}\mathbf{y} + \mathbf{h}^\varepsilon(\mathbf{T}\mathbf{y})) + \varepsilon\mathbf{F}(\mathbf{x} + \mathbf{h}^\varepsilon(\mathbf{T}\mathbf{y}), t),$$

which can be rearranged as

$$\begin{aligned} \dot{\mathbf{y}} &= (\mathbf{T} + D\mathbf{h}^0(\mathbf{T}\mathbf{y})\mathbf{T} + O(|\mathbf{y}|\varepsilon))^{-1} [\mathbf{A}(\mathbf{T}\mathbf{y} + \mathbf{h}^0(\mathbf{T}\mathbf{y}) + O(|\mathbf{y}|^2\varepsilon))] \\ &+ (\mathbf{T} + D\mathbf{h}^0(\mathbf{T}\mathbf{y})\mathbf{T} + O(|\mathbf{y}|\varepsilon))^{-1} \left[\tilde{\mathbf{f}}(\mathbf{T}\mathbf{y} + \mathbf{h}^0(\mathbf{T}\mathbf{y}) + O(|\mathbf{y}|^2\varepsilon)) + \varepsilon\mathbf{F}(\mathbf{T}\mathbf{y} + \mathbf{h}^0(\mathbf{T}\mathbf{y}), t) \right]. \end{aligned} \quad (104)$$

Since $y + h^0(y)$ linearizes (52) for $\varepsilon = 0$, (104) simplifies to

$$\dot{\mathbf{y}} = \boldsymbol{\Lambda}\mathbf{y} + (\mathbf{T} + D\mathbf{h}^0(\mathbf{T}\mathbf{y})\mathbf{T})^{-1}\varepsilon\mathbf{F}(\mathbf{0}, t) + O(|\mathbf{y}|^2\varepsilon, \mathbf{y}\varepsilon^2), \quad \mathbf{y} = (\boldsymbol{\xi}, \boldsymbol{\eta})^T. \quad (105)$$

The smoothest SSM $\mathcal{W}_\varepsilon(E, t)$ of the periodic orbit is $O(\varepsilon)$ -close to that of the fixed point and can be written as

$$\mathcal{W}_\varepsilon(E, t) = \begin{pmatrix} \boldsymbol{\xi} \\ O(\varepsilon) \end{pmatrix}.$$

We now neglect the small, time-dependent correction to the $\boldsymbol{\eta}$ -component of $\mathcal{W}_\varepsilon(E, t)$. The reduced dynamics can then be written as the projection of (105) to the $\boldsymbol{\eta} = 0$ plane, which becomes

$$\dot{\boldsymbol{\xi}} = \boldsymbol{\Lambda}_E\boldsymbol{\xi} + (\mathbf{T} + D\mathbf{h}^0(\mathbf{T}\mathbf{y})\mathbf{T})^{-1}|_E\varepsilon\mathbf{F}(\mathbf{0}, t) + O(|\mathbf{y}|^2\varepsilon, \mathbf{y}\varepsilon^2), \quad \boldsymbol{\Lambda}_E = (\mathbf{T}^{-1}\mathbf{A}\mathbf{T})|_E. \quad (106)$$

The restriction of the observable vector $\boldsymbol{\phi}$ to the subspace E can be written as $\boldsymbol{\varphi}(\boldsymbol{\xi})$. Repeating the arguments of D, the change of coordinates $\boldsymbol{\xi} = \boldsymbol{\psi}(\boldsymbol{\varphi})$ can be carried out, which transforms (106) to

$$\dot{\boldsymbol{\varphi}} = D_{\boldsymbol{\xi}}\boldsymbol{\varphi}(\mathbf{0})\boldsymbol{\Lambda}_E [D_{\boldsymbol{\xi}}\boldsymbol{\varphi}(\mathbf{0})]^{-1} \boldsymbol{\varphi} + \mathbf{q}(\boldsymbol{\varphi}) + \varepsilon \left\{ \left[\mathbf{I} + D\mathbf{h}^0(D_{\boldsymbol{\xi}}\boldsymbol{\varphi}(\mathbf{0}))^{-1} \right] \mathbf{T}_E \right\}^{-1} \mathbf{F}(\mathbf{0}, t) + O(|\boldsymbol{\varphi}|^2\varepsilon, |\boldsymbol{\varphi}|\varepsilon^2), \quad (107)$$

$$\mathbf{q}(\boldsymbol{\varphi}) = o(|\boldsymbol{\varphi}|),$$

which proves formula (53).

F Forced response from approximate DDL

As stated in Section 4.3.4, the linearizing change of coordinates $\varphi = \kappa(\gamma) = \gamma + \ell(\gamma)$ transforms the reduced dynamics of the forced system (107) to the form $\dot{\gamma} = \mathbf{B}\gamma + \varepsilon(\mathbf{I} + D\ell(\gamma))^{-1}\hat{\mathbf{F}}(\mathbf{0}, t)$. Therefore, a trajectory of the forced system may be computed by integrating (55) and transforming to the reduced coordinates φ as

$$\varphi(t) = \gamma(t) + \ell(\gamma(t)).$$

An approximate version of (55) may be obtained by assuming (56), i.e., $\varepsilon(\mathbf{I} + D\ell(\gamma))^{-1} = \varepsilon\mathbf{I} + O(\varepsilon|\gamma|) \approx \varepsilon\mathbf{I}$. This results in the forced linear system

$$\dot{\gamma} = \mathbf{B}\gamma + \varepsilon\hat{\mathbf{F}}(\mathbf{0}, t). \quad (108)$$

However, we must keep in mind that the $O(\varepsilon|\gamma|)$ terms are already retained when we compute $\varphi(t) = \gamma(t) + \ell(\gamma(t))$, therefore terms of the same order must also be retained in the dynamics (55). Nevertheless, assumption (56) makes the dynamics (108) an inhomogeneous linear system of ODEs, which is simple to solve. We refer to DDL under assumption (56) as Approximate DDL. We compare forced response predictions of the analytic linearization, DDL, Approximate DDL and DMD on the forced-damped Duffing system discussed in Section 5.3.

In Fig. 12, we repeat the results already presented in Fig. 6, which should now be compared to the forced response predicted using Approximate DDL. Panel (a) shows that although Approximate DDL is accurate only for low amplitudes, it clearly outperforms the DMD-model. For higher amplitudes, predictions are not accurate, since the forced linear system (108), by construction, cannot show nonlinear behavior. In contrast, the analytic linearization and the full DDL continue to yield accurate predictions for the forced response, even in the nonlinear regime.

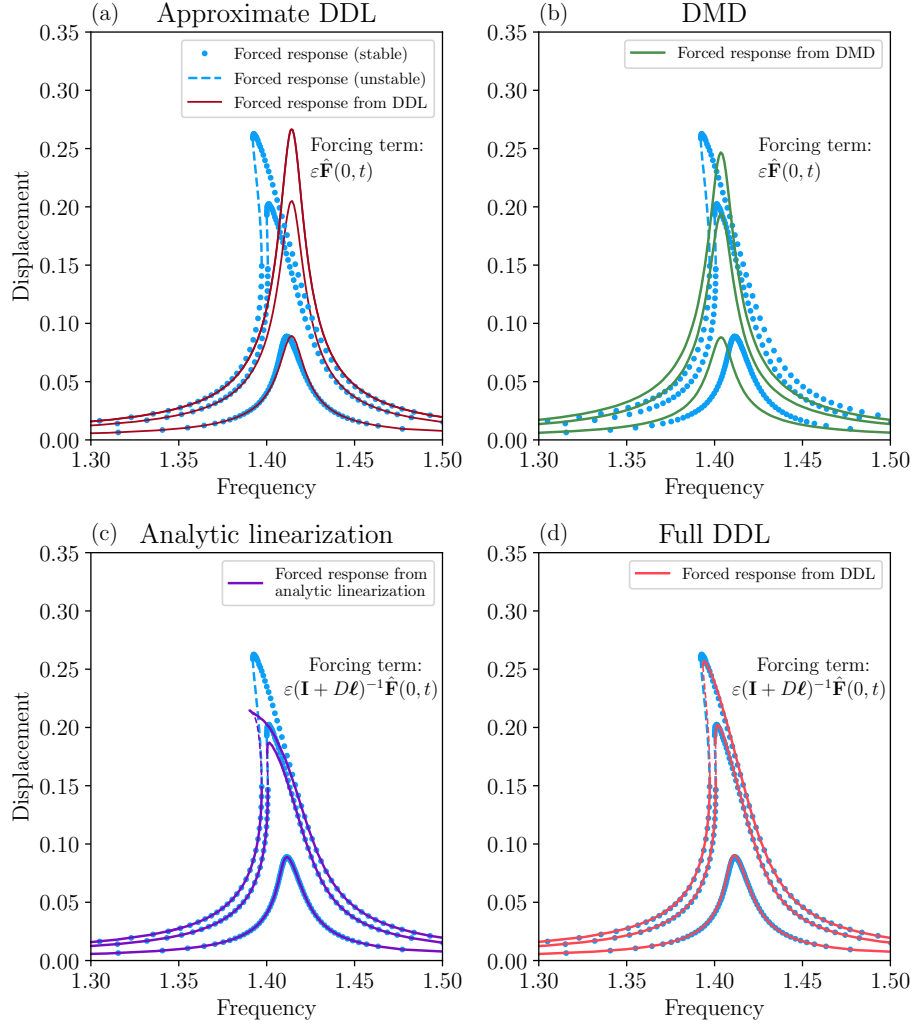


Figure 12: Periodic response of the forced Duffing oscillator (63). Panel (a) shows DDL-predictions under the simplifying assumption (56). Panels (b)-(d) are the same as Fig. 6.